

Submitted to ApJ

Observations of T-Tauri Stars using HST-GHRS: I. Far Ultraviolet Emission Lines

David R. Ardila¹, Gibor Basri², Frederick M. Walter³, Jeff A. Valenti⁴, Christopher M. Johns-Krull⁵

ABSTRACT

We have analyzed GHRS data of eight CTTS and one WTTS. The GHRS data consists of spectral ranges 40 Å wide centered on 1345, 1400, 1497, 1550, and 1900 Å. These UV spectra show strong Si IV, and C IV emission, and large quantities of sharp (~ 40 km s $^{-1}$) H₂ lines. All the H₂ lines belong to the Lyman band and all the observed lines are single peaked and optically thin. The averages of all the H₂ lines centroids for each star are negative which may indicate that they come from an outflow. We interpret the emission in H₂ as being due to fluorescence, mostly by H_{Lyα} and identify seven excitation routes within 4 Å of that line. We obtain column densities (10^{12} to 10^{15} cm $^{-2}$) and optical depths (~ 1 or less) for each exciting transition. We conclude that the populations are far from being in thermal equilibrium. We do not observe any lines excited from the far blue wing of H_{Lyα}, which implies that the molecular features are excited by an absorbed profile. Si IV and C IV (corrected for H₂ emission) have widths of ~ 200 km s $^{-1}$, and an array of centroids (blueshifted lines, centered, redshifted). These characteristics are difficult to understand in the context of current models of the accretion shock. For DR Tau we observe transient strong blueshifted emission, perhaps the a result of reconnection events in the magnetosphere. We also see evidence of multiple emission regions for the hot lines. While C IV is optically thin in most stars in our sample, Si IV is not. However, C IV is a good predictor of Si IV and H₂ emission. We conclude that most of the flux in the hot lines may

¹Astronomy Dept., Univ. of California, Berkeley, CA 94720, ardila@garavito.berkeley.edu

²Astronomy Dept., Univ. of California, Berkeley, CA 94720, basri@soleil.berkeley.edu

³Department of Physics and Astronomy, SUNY, Stony Brook NY 11794-3800, fwalter@astro.sunysb.edu

⁴Space Telescope Science Institute, Baltimore, MD 21218, valenti@stsci.edu

⁵Space Sciences Laboratory, Berkeley, CA 94720, cmj@ssl.berkeley.edu

be due to accretion processes, but the line profiles can have multiple and variable components.

Subject headings: stars: pre-main-sequence — stars: winds, outflows — stars: formation — stars: BP Tauri, T Tauri, DF Tauri, RW Aurigae, DG Tauri, DR Tauri, RY Tauri, RU Lupi, HBC 388 — ultraviolet: stars

1. Introduction

The peculiar spectral characteristics of Classical T Tauri stars (CTTSs) are usually interpreted as the result of a circumstellar disk accreting onto a magnetized young star. Considerable development of this idea has occurred during the last decade. The current paradigm asserts that the inner region of the disk is truncated by the stellar magnetic field and partially ionized material slides down to the stellar surface. Close to the surface the gas produces a strong shock, in which the kinetic energy of the infalling stream is transformed into random thermal motions. It is thought that radiation from the shock reprocessed by the stellar surface is responsible for the UV and optical continuum excess ('veiling'). This process has been modeled in detail by Calvet & Gullbring (1998) and Gullbring, Calvet, Muzeolle, & Hartmann (2000), who use the strength of the ultraviolet continuum to obtain accretion rates and spot sizes for CTTS.

Given the high temperature of the gas in the inner stellar magnetosphere, wavelengths shorter than the Balmer jump contain important spectral diagnostics. For material infalling at $\sim 300 \text{ km s}^{-1}$, the strong shock conditions imply a shock temperature of $\sim 10^6 \text{ K}$, which decreases monotonically as the gas settles onto the star (Calvet & Gullbring 1998). With densities ranging from 10^{10} cm^{-3} to 10^{14} cm^{-3} (depending on the accretion rate, area of the accretion column and the specific model), the region is similar to the chromosphere, transition region, and corona of the underlying star. Even though the physics involved is very different, one expects to observe transition region diagnostics, like C IV at 1550 \AA (which, when it is collisionally dominated in the low density limit, has maximum population at 10^5 K , see Arnaud & Raymond 1992) and Si IV at 1400 \AA (formed at 63000 K in the same limit), and chromospheric diagnostics such as the Mg II resonance doublet at 2800 \AA .

Analyses of low-resolution observations by the International Ultraviolet Explorer (IUE) suggest that a large fraction of the C IV emission does indeed come from processes related to accretion (as opposed to intrinsic transition region emission). Johns-Krull, Valenti, & Linsky (2000) have shown that the flux in the C IV resonance doublet is up to two orders of magnitude larger than in main-sequence and RS CVn stars with the same dynamo number

(a measure of magnetic activity). Furthermore, such emission is well correlated with the estimates of accretion rates obtained from optical data (Hartigan, Edwards, & Ghandour 1995). On the other hand, as Johns-Krull et al. (2000) argue, due to the different internal structure of T-Tauri Stars (TTSs) compared to these other stars, it is not clear what fraction of the line is due to accretion as opposed to other possible sources. Even though the evidence that supports the connection between accretion and large transition region line emission is strong, it is not conclusive.

If due to accretion, the line shapes of the transition lines should reflect the conditions in the accretion shock. Gomez de Castro, Lamzin, & Shatskii (1994) have studied the C IV and Si IV lines using high resolution observations of CTTS by IUE. They argue that the profiles of these lines should have at least two distinct peaks: one due to emission coming from the pre-shock zone and another from emission coming from material immediately after the shock. Another emission peak may appear, due to shocked material close to the star. Such prediction has been formalized in the models developed by Lamzin (1998). Given the low signal-to-noise of the IUE observations, it is not clear to what extent these two and three-peaked profiles are actually observed.

Semiforbidden ultraviolet line ratios have been used (Johns-Krull et al. 2000; Gomez de Castro & Lamzin 1999; Lamzin 2000c) to estimate the density of the shocked material. Johns-Krull et al. (2000) show that the density of the shock, as measured by these ratios, is 3 to 4 orders of magnitude less than the densities assumed in the models by Calvet & Gullbring (1998) but coincide with the densities predicted by Lamzin (1998). Theoretically, the shock density depends on parameters that are not well determined, such as the accretion rate, the reddening of the star, and the covering fraction of the shock.

Comparing observations of C IV and Si IV lines to models is complicated by the fact that the UV spectra of TTSs show strong H₂ emission lines, and some of those are blended with the doublets. The H₂ lines were first identified by Brown et al. (1981) and Brown, de M. Ferraz, & Jordan (1984) in T Tau. Based on IUE low-resolution spectra, they suggest that the lines are the result of resonant fluorescence of molecular hydrogen (excitation from $X^1\Sigma_g^+$ to $B^1\Sigma_u^+$, the Lyman band) by H_{Ly α} . The H₂ line R(3)1-8 is at -166 km s^{-1} from the red member of the C IV doublet and therefore it alters its profile. The same is true for Si IV and the H₂ lines R(0)0-5 (at -8 km s^{-1}), R(1)0-5 (at $+44 \text{ km s}^{-1}$), and P(3)0-5 (at -25 km s^{-1}). In the Sun, Si IV and C IV have themselves been identified as pumping mechanisms for H₂ (Jordan et al. 1978; Bartoe et al. 1979).

H₂ ultraviolet emission has also been identified in the large sample of TTSs presented by Valenti, Johns-Krull, & Linsky (2000). At least in the case of T Tau, the emission is extended more than 5 arcsecs (Brown et al. 1981; Herbst, Robberto, & Beckwith 1997),

and has a very complex structure which includes filaments and knots (van den Ancker et al. 1999).

The analysis of H₂ observations in CTTSs has centered around the heating mechanism for the molecule, and the origin of the emission (either the disk or nebular material surrounding CTTSs). As H₂ is supposed to be the most abundant species in a TTS system, analysis of its physical conditions has important implications for a wide range of topics, from the gas-disk dissipation timescale to the characteristics of the outflow. While a lot of work has been done about the observational characteristics of the infrared H₂ emission (e.g. Thi et al. 1999; van Dishoeck et al. 1997; Herbst, Robberto, & Beckwith 1997), relatively little work has been published regarding the ultraviolet fluorescent lines in the context of CTTS (Lamzin, Vittone, & Errico 2001; Black & van Dishoeck 1987; Walter & Liu 1998), perhaps because of the scarcity of high-resolution observations of the fluorescent lines. ISO observations of the far IR H₂ lines of T Tauri (van den Ancker et al. 1999) reveal two different components of different temperatures (500 and 1500 K) contributing to the emission. Furthermore, while the bulk of the heating is due to shocks (either from the outflow against the ISM or from infalling material into the disk of T Tau S), the signature of fluorescence processes is observed, even in the IR lines from low-lying states. In the context of the UV lines, Walter & Liu (1998) have shown, using low-resolution GHRS observations, that one can generally detect H₂ emission from CTTSs, while none is detected in Weak T Tauri Stars (WTTSs). By assuming that the observed H₂ comes from the disk, they conclude that the gas-disk dissipation timescale is similar to the dust-disk dissipation timescale.

Most of the ultraviolet observations of TTSs have been performed with IUE. In spite of the prodigious amount of data this spacecraft produced, observations of TTSs suffered from its small aperture and the low sensitivity (by today's standards) of its Vidicom cameras. This situation improved with the launch of the Goddard High Resolution Spectrograph (GHRS), which flew on board the Hubble Space Telescope from 1990 to 1997; however, only a handful of TTSs were observed with this instrument.

The objective of the present work is to describe the main features of the ultraviolet range (mainly in two windows 40 Å wide centered on 1400 and 1550) for a sample of eight CTTSs and one WTTS. The data were obtained with the GHRS instrument in the early 1990s. A portion of these data has been independently analyzed (Errico, Lamzin, & Vittone 2000; Lamzin 2000a,b,c; Lamzin et al. 2001). It has also been described in conference reports (Calvet et al. 1996; Valenti et al. 1993). The main features in these spectra are the Si IV and C IV resonance doublets, and strong H₂ lines. In a companion paper we analyze the Mg II resonance doublet, part of this same set of data.

The remainder of this paper is organized as follows: We start with a description of the

observations. In section 3 we comment on the general characteristics of the data. In section 4.1 we analyze the characteristics of the H₂ lines present in the spectra. As mentioned above, some of these lines are blended with C IV and Si IV. In section 4.2 we indicate how to obtain unblended profiles for the resonance doublets. Section 4.3 contains an analysis of the unblended profile. Our conclusions are in section 5.

2. Observations

The characteristics of the observed targets are summarized in Table 1. All (except RU Lupi) belong to the Taurus star formation region, and we assume that all are at a mean distance of 140 pc from the Sun. The target stars have a range of accretion rates and include a weak TTS (WTTS), HBC 388 (other names are V1072 Tau and NTTs 042417+1744). This star does not show IR excess that could be attributed to a circumstellar disk (Wolk & Walter 1996) and its $H\alpha$ line is very weak (Walter et al. 1988). Therefore, spectral diagnostics related to the accretion process are expected to be negligible, and its emission can be assumed to be due only to magnetic-related phenomena (chromosphere, transition region, and corona).

As indicated in Table 1, there are three multiple systems in the sample. In each case, all members of the system are within the slit. For DF Tau, both components have similar brightness. Speckle observations of the system suggest that it is composed of a CTTS and a WTTS. The orbital inclination from these observations is estimated to be $i \sim 65^\circ$ (Thiebaut et al. 1995), consistent with the $\sim 80^\circ$ derived from analysis of variability. The companion of T Tau N is a very embedded young object, with a circumstellar disk. Reports of a third member of the system remain unconfirmed (Stapelfeldt et al. 1998). RW Aur ABC is a triple system, with a factor of 10 difference in luminosity between the primary (A) and the secondary (BC) (Ghez, White, & Simon 1997). We unpublished high resolution spectra that suggest that RW Aur B is possibly a very weak K7 CTTS.

In Table 1 we use mostly the reddenings and accretion rates from Gullbring et al. (1998), Calvet & Gullbring (1998), and Gullbring et al. (2000) (GCHB). RW Aur, RY Tau, and RU Lup do not have these values measured in those works. For RW Aur and RY Tau we use the extinction values determined by Johns-Krull et al. (2000). In general, accretion rates determined by GCHB are one order of magnitude less than those determined by Hartigan et al. (1995) (HEG95). Therefore, for RY Tau and RW Aur we have divided the accretion rate from HEG95 by 10, to obtain the values quoted in the Table. Note that the value for the reddening of RU Lup is taken from Hughes et al. (1994) and the accretion rate is taken from Johns-Krull et al. (2000). The accretion rates divide the CTTS sample in three subsets: stars with low (RY Tau), ‘average’ (BP Tau, T Tau), and high accretion rate.

2.1. UV Observations

We obtained these data using the Goddard High Resolution Spectrograph (GHRS; see Brandt et al. 1994), one of the first generation instruments aboard the Hubble Space Tele-

Table 1. Parameters of Observed Stars

Name	Spectral Type	Class	R_* (R_\odot)	M_* (M_\odot)	A_V^a (mag)	\dot{M}^b ($10^{-8} M_\odot/yr$)	V_r^c (km/s)	Inclination ^d (deg)	Multiplicity ^e
BP Tauri	K7	CTTS	2.0	0.5	0.51	2.88	15.8 ^f	< 50	S ^g
T Tauri NS	K0	CTTS	3.4	2.0	1.7	4.00	19.1 ^f	20	M (0.7") ^g
DF Tauri AB	M0	CTTS	3.4	0.3	0.45	17.7	15.8 ^h	80	M (0.09") ⁱ
RW Aurigae ABC	K4	CTTS	1.4 ^j	1.1 ^j	1.14	16	16 ^k	40	M (1.5") ^g
DG Tauri	K5	CTTS	2.3	0.7	1.6	50	15.9 ^h	40 ^l	S ⁱ
DR Tauri	K7	CTTS	2.7	0.4	1.2	30	27.6 ^m	<40	S ⁱ
RY Tauri	K1	CTTS	2.4	1.6	0.29	0.25	16.4 ^f	90	S ⁱ
RU Lupi	K7	CTTS	3.2	0.3	1.28 ⁿ	77 ^o	-0.5 ^f	0 ^p	S ^p
HBC 388	K1 ^q	WTTS	1.5	1.3	0.1	...	15.4	45 ^r	S ⁱ

Note. — The data for this table were taken from Johns-Krull et al. (1999), Table 1, unless indicated otherwise.

^aFrom GHBC for all except RW Aur and RY Tau. For these two, the values are from Johns-Krull et al. (1999)

^bFrom GHBC for all except RW Aur and RY Tau. For these two, we have taken the HEG95 values and divided by 10.

^cHeliocentric velocity

^dUnless otherwise indicated, it is calculated from $v \sin i$ and P_{rot} values quoted by Johns-Krull et al. (2000). Rounded to one significant figure.

^eS=single, M=Multiple, the number indicates the separation

^fHerbig & Bell (1988)

^gLeinert et al. (1993)

^hHartmann et al. (1991)

ⁱGhez, Neugebauer, & Matthews (1993)

^jPetrov et al. (2001)

^kGahm et al. (1999)

^lBacciotti et al. (2000)

^mAlencar & Basri (2000)

ⁿHughes et al. (1994)

^oJohns-Krull et al. (2000), Table 4. Obtained via a correlation between accretion rate and CIV.

^pLamzin et al. (1996)

^qUnless otherwise indicated the data for this line come from Walter et al. (1988)

^r $P_{rot} = 2.74d$ from Preibisch & Smith (1997). $v \sin i = 20$ from Sartoretti et al. (1998)

scope.

The GHRS is a modified Czerney-Turner spectrograph with Digicon detectors. The in-orbit performance of the GHRS is described by Heap et al. (1995). These data were obtained in GO programs executed in cycles 3 and 5, as well in GTO observations in cycles 2 and 3. Table 2 presents the log of observations.

Table 2. Log of Observations

Target Date	λ_{cen} (Å)	UT start (UT)	Exposure (sec.) (sec.)	Readouts	Root
Pre-COSTAR					
RU Lup 8/24/92	1400.6	3:18:59	768	3	Z10T0104
	1549.7	3:34:38	1280	5	Z10T0105
	1640.3	4:43:59	1280	5	Z10T0107
	1899.5	5:10: 8	1408	5	Z10T0109
	2324.7	6:26:50	512	2	Z10T010C
BP Tau 7/30/93	1400.8	17:54:11	1689	6	Z18E0107
	1550.0	19:12:58	1408	5	Z18E0108
RW Aur 8/10/93	1400.8	22:13:41	844	3	Z18E0407
	1550.0	23:20:25	844	3	Z18E0408
DR Tau 8/5/93	1400.8	0:53:29	1689	6	Z18E0307
	1550.0	2:15:25	1689	6	Z18E0308
	1345.8	3:44:19	1408	5	Z18E0309
	1650.4	4:12: 7	1126	4	Z18E030B
DF Tau 8/8/93	1400.8	2:50:41	1126	4	Z18E0207
	1550.0	4:10:34	1126	4	Z18E0208
	1345.8	5:37: 4	1408	5	Z18E0209
RY Tau 12/31/93	1400.6	4:25:51	1024	4	Z1E70104
	1549.8	5:52:21	1280	5	Z1E70105
	1640.4	7:16:40	1280	5	Z1E70106
	1899.6	7:42:36	1408	5	Z1E70108
Post-COSTAR					
DR Tau	1552.9	18: 2:53	5632	20	Z2WB0207

All observations before 1994 were made using the aberrated optics; later observations used the COSTAR corrective optics¹. The pre-COSTAR data are not seriously affected by the mirror aberrations, because of the combination of broad lines and (generally) low S/N per pixel, so we made no effort to deconvolve the aberrated line profile.

Target acquisitions occurred in the N2 mirror, using a 3×3 spiral search pattern. For the cycle 5 observations we used the BRIGHT=RETURN option. Dwell times ranged from 0.2 to 2.0 seconds; count rates ranged from 1200 to 8000 counts s^{-1} . All targets were successfully acquired. Exposure times in Table 2 reflect the time observing the target, excluding the time spent exposing background.

All observations were obtained through the large science aperture, which projects to a 2 arcsec square on the sky pre-COSTAR, and to 1.74 arcsec post-COSTAR. We used substep pattern 5 (four on-target observations offset by $\frac{1}{4}$ diode, and two background observations with the detector array deflected above and below the spectrum) for all observations. The four on-target observations were summed using comb-addition (see Heap et al. 1995). Each pixel corresponds to $\frac{1}{4}$ diode width; the instrumental resolution is about 4.4 pixels. The large science aperture subtends 8 diodes, or 32 pixels, in the dispersion direction. The instrumental resolution is constant with wavelength and is the same for each individual observation and the co-added frame. The resolving power is 20000 at 1500 Å.

All observations utilized the side 2 (long wavelengths) optics with the CsTe Digicon detector and the medium wavelength gratings (G160M, G200M, G270M). To minimize the effect of GIMP-induced image motions, all observations were read out about every 5 minutes. No significant drifts were seen.

2.1.1. *GHRS Data Reduction*

We converted the spectra from GEIS format to GHRS format data files using the HRS_ACQUIRE software (Blackwell et al. 1993). The data were extracted and calibrated using version 2.20 of the IDL-based CALHRS software (Brandt et al. 1993) with the default calibration files appropriate for the dates of the observations.

Because our targets are not bright and most of the flux in the ultraviolet is in emission lines, proper background subtraction is crucial. The GHRS background is primarily due to passage of cosmic rays through the Digicon window. The mean background rates vary with

¹Although the RY Tau observations on 1993 December 31 occurred after the installation of COSTAR, they occurred before the GHRS corrective optics were deployed.

geomagnetic latitude, and exhibit non-Poisson fluctuations. Cosmic ray events are characterized by enhanced counts affecting a number of contiguous diodes. Because the integration time on the background is significantly less than that on the target, the background rates are much more sensitive to these bursts of counts from cosmic rays.

We examined all pairs of background bins for evidence of non-Poissonian fluctuations. In those cases where the background count rates differed by more than 5σ , we replaced the affected substep bin with the rate from the other background bin. Retention of the high background bins had resulted in negative continua in some cases. We then subtracted a uniform mean background rate (this is the same as fitting the background with a zero-order polynomial).

2.1.2. *Wavelength Calibration*

The default dispersion solution, based on the carrousel position, is expected to be accurate to ± 0.1 diodes. To verify accuracy of the wavelength scale, we obtained WAVECAL observations as part of eight of the observations. No WAVECAL exposures accompany the RU Lup or RY Tau observations. In the second DR Tau observation the WAVECAL accompanied the C IV observation, in all other cases it preceeded the Si IV observation. For all observations not preceeded by a WAVECAL observation, we used the preceeding SPYBAL² observation to determine zero-point of the wavelength scales.

To verify the internal accuracy of the wavelength scales, we also reduced those observations preceeded with WAVECAL observations with the preceeding SPYBAL observation and compared the wavelength scales. The mean offsets are 0.3 ± 1.0 diodes (1.0 ± 3 km s⁻¹), where the uncertainty is the RMS deviation in the measurements. This can be taken as a representative statistical uncertainty on the wavelength scale. There may be systematic offsets of up to ± 6 pixels (± 20 km s⁻¹) due to the target centering process, primarily for the pre-COSTAR observations. Further offsets may result from non-uniform filling of the aperture in the case of extended emission.

All readouts from a particular observation were then interpolated to a common linear wavelength scale and summed. An effect of the interpolation is to smooth the data, and we scaled the error vectors accordingly.

²The SPYBAL (spectral Y-balance) is a WAVECAL observation at a default carrousel position which is performed whenever the grating is changed in order to center the spectrum on the Digicon array. WAVECAL observations are made at the same carrousel position as the following observation.

3. General Characteristics

Figures 1 to 7 show our ultraviolet data. All the spectra plotted are in the stellar rest frame. Spectra centered around the same wavelength are grouped together. To facilitate line identifications, the spectra have been convolved with a Gaussian having $\text{FWHM}=0.072 \text{ \AA}$ (four pixels). For each spectrum we mark the lines for which we measure a flux. Note that in the spectra of RU Lup one bad diode was not properly accounted for at the time these data were reduced. We have zeroed the affected points.

The main features of the UV spectra are the Si IV (1393.755, 1402.770 \AA) and C IV (1548.187, 1550.772 \AA) resonance doublets. In both doublets the blue member has an f -value that is twice that of the red member. All doublet lines are fairly wide (~ 150 to $\sim 300 \text{ km s}^{-1}$) and show a wide array of shapes and fluxes, from the very symmetric broad peaks of BP Tau to the narrow peaks (in Si IV) and blueshifted features (in C IV) for DG Tau.

Atomic lines from other species (O I] and C II) are also present in emission for some of the spectra. They indicate the presence of an extended low temperature plasma. Although C II is blended with a group of H_2 lines which make its analysis difficult, it is clear that these low temperature lines show blueshifted absorption, probably due to the stellar wind. The data do not have enough signal-to-noise to characterize these lines very precisely.

Most of the spectra show conspicuous H_2 features, which blend with the Si IV and C IV lines, as indicated in the introduction. The exception is HBC 388, for which only the peaks of the Si IV and C IV lines are significant above the noise. All the detected H_2 transitions correspond to the Lyman Band. The lines are generally sharp ($\text{FWHM} \sim 40 \text{ km s}^{-1}$).

4. Analysis

As indicated below, we have measured the parameters of H_2 , C IV and Si IV. The results are shown in Table 3. For each measurement we have used the noise vector provided with the data to obtain an error estimate. The numbers in Table 3 without error estimates are deduced from other parameters.

In general, we have measured fluxes, full widths at half-maxima, and velocity shifts, by fitting a Gaussian or a combination of Gaussians to the profiles, using a Marquardt routine. The fits have been done on the unsmoothed spectra. For some stars we perform line decomposition in terms of a broad component (BC) and a narrow component (NC). For DF Tau, we decompose each member of the C IV doublet in three components labeled C1, C2, C3. The H_2 lines are grouped lines that originate in the same upper v' , J' level. We

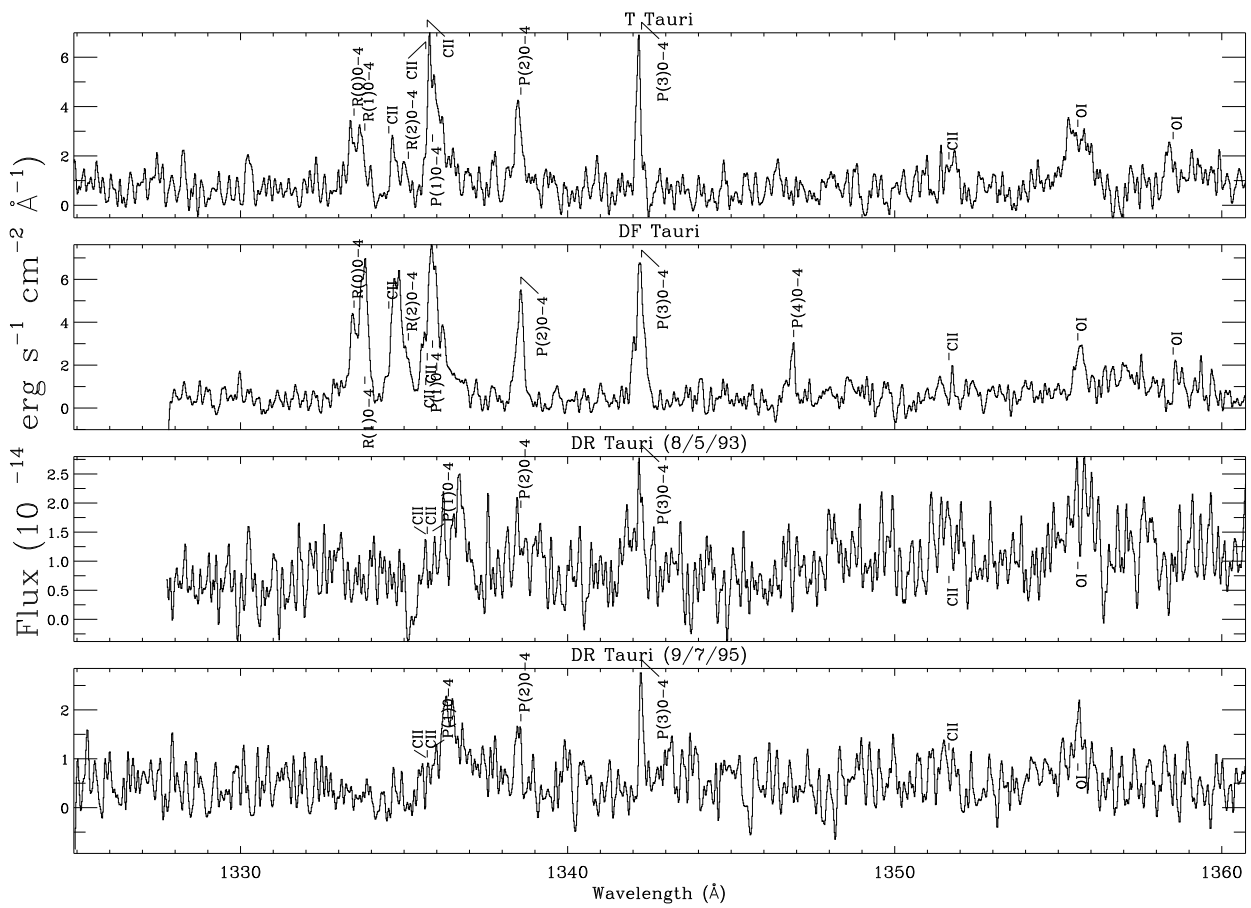


Fig. 1.— Smoothed spectra centered around 1342 Å.

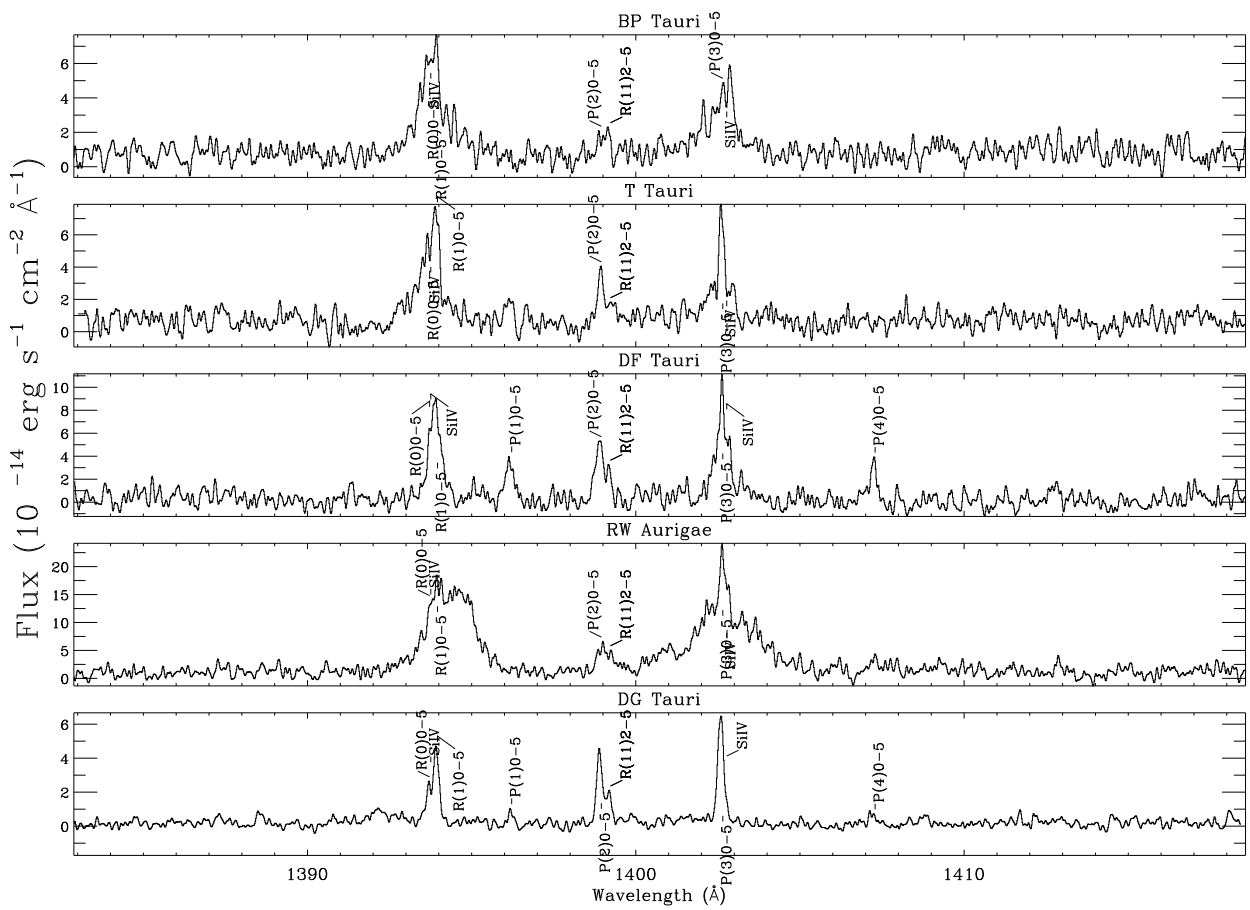


Fig. 2.— Smoothed spectra centered around 1400 Å. This region contains the Si IV doublet.

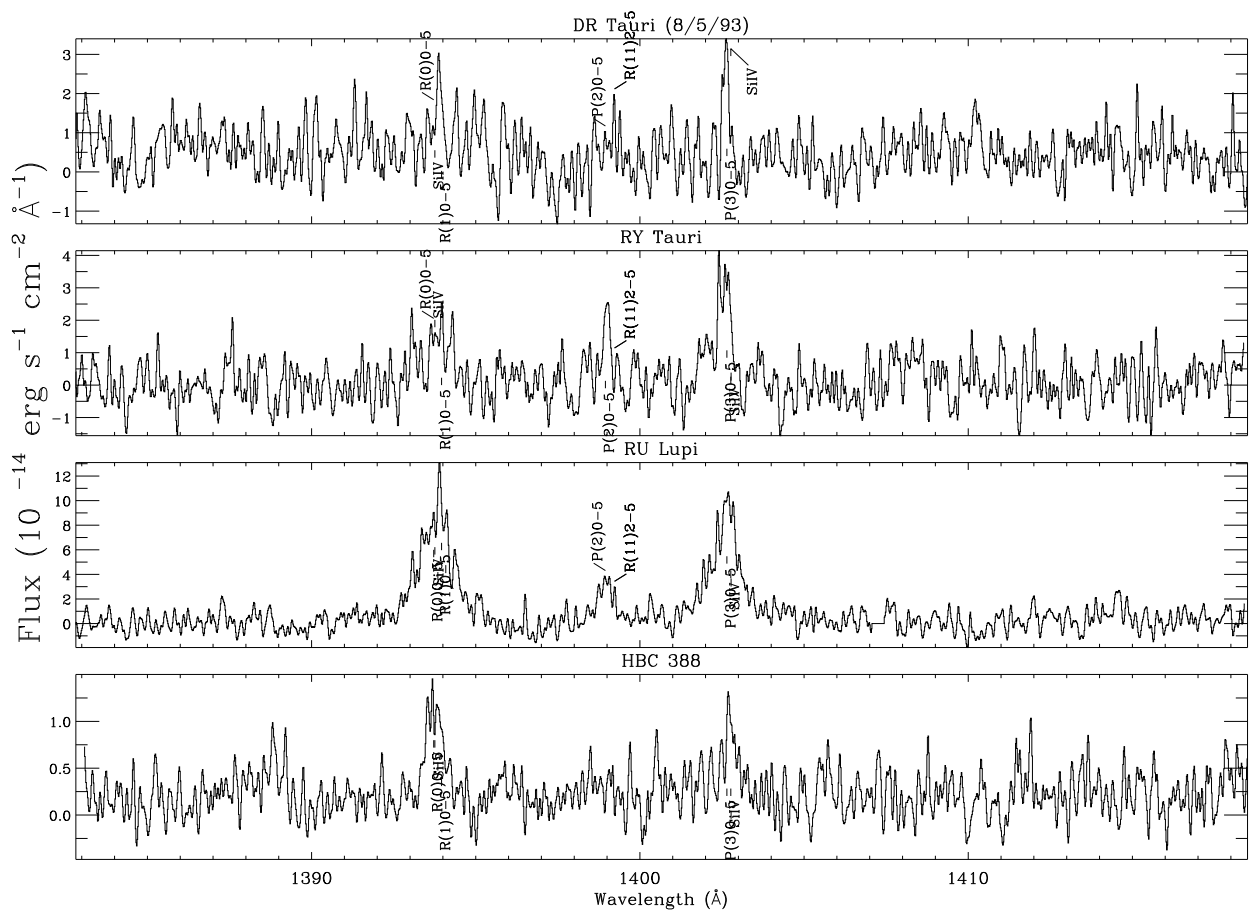


Fig. 3.— Smoothed spectra centered around 1400 Å, cont.

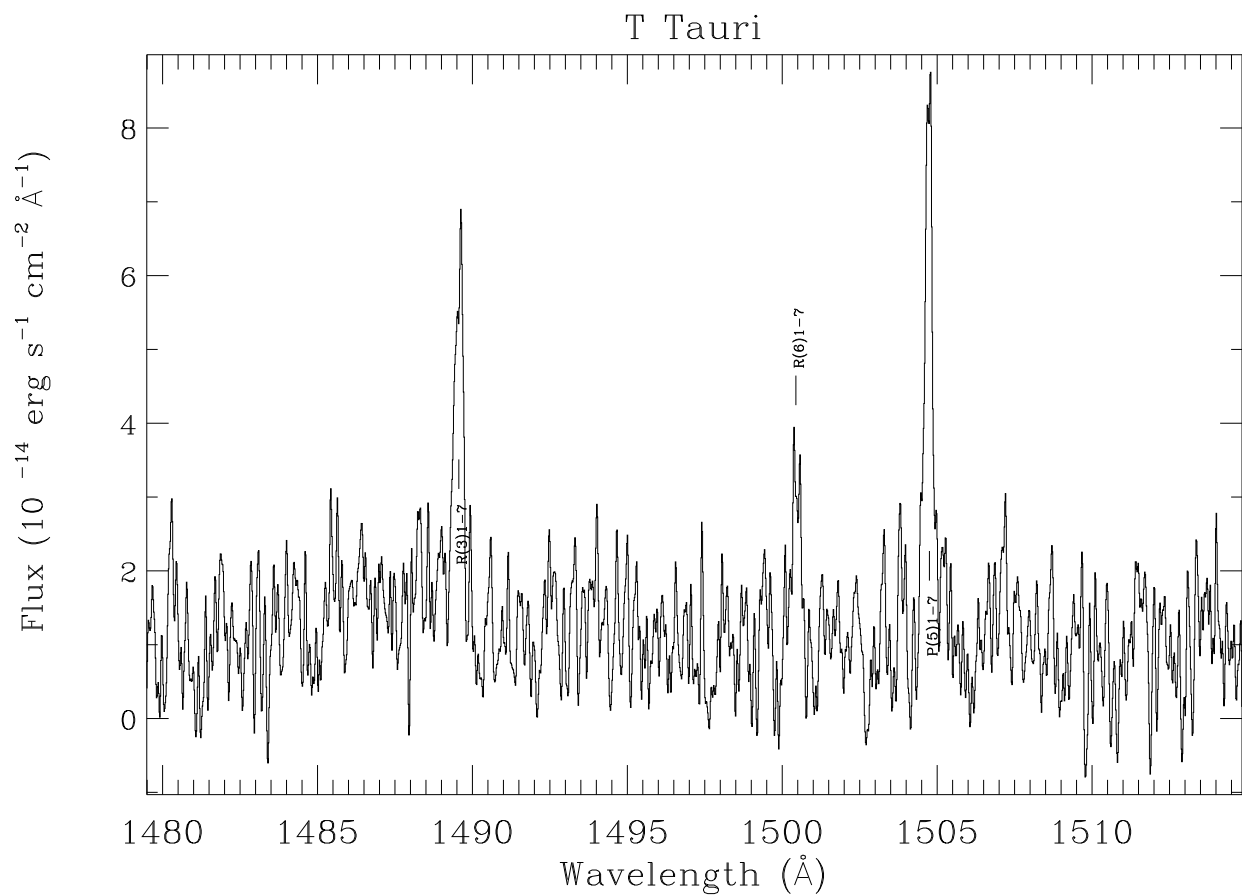


Fig. 4.— We only have one spectrum centered around 1500Å.

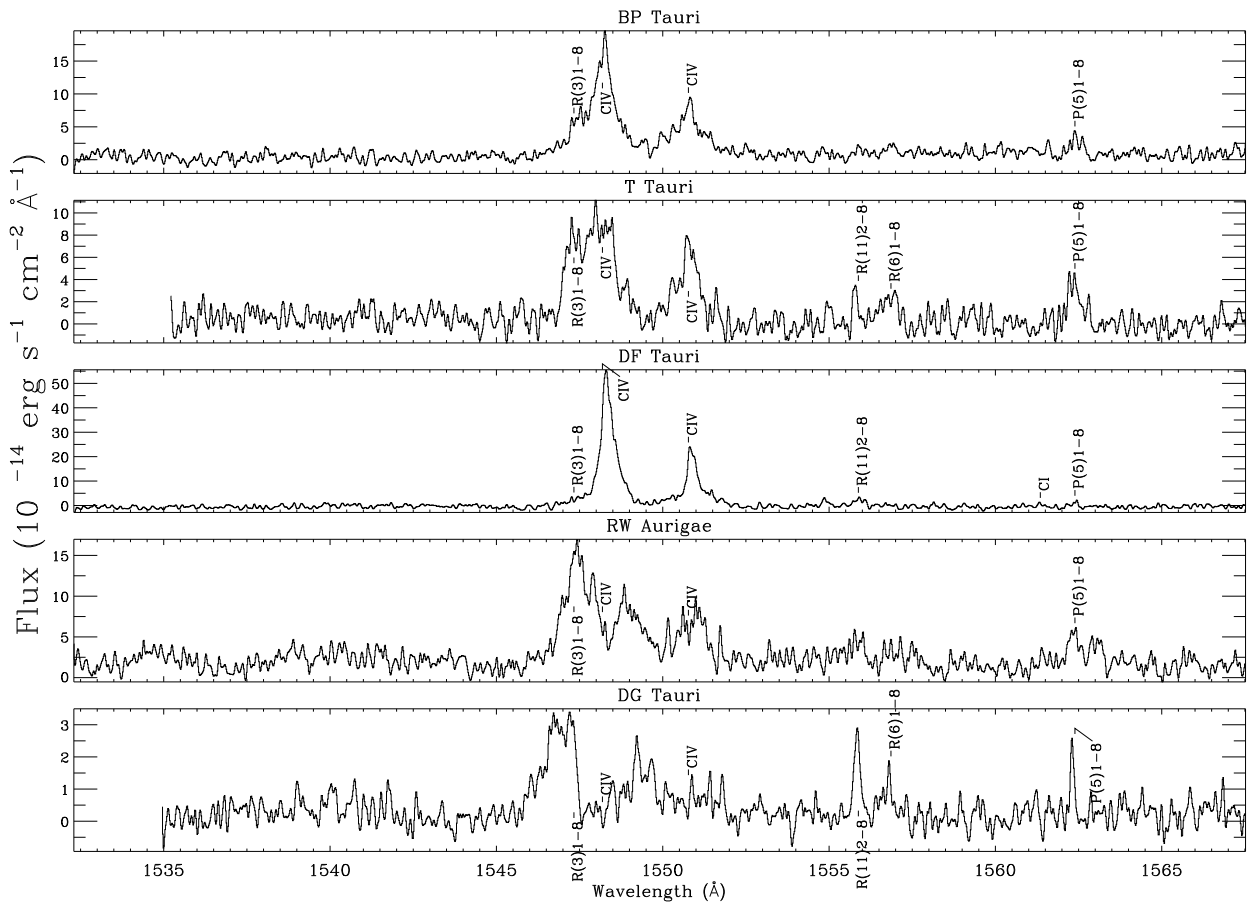


Fig. 5.— Smoothed spectra centered around 1550 Å. This region contains the C IV doublet.

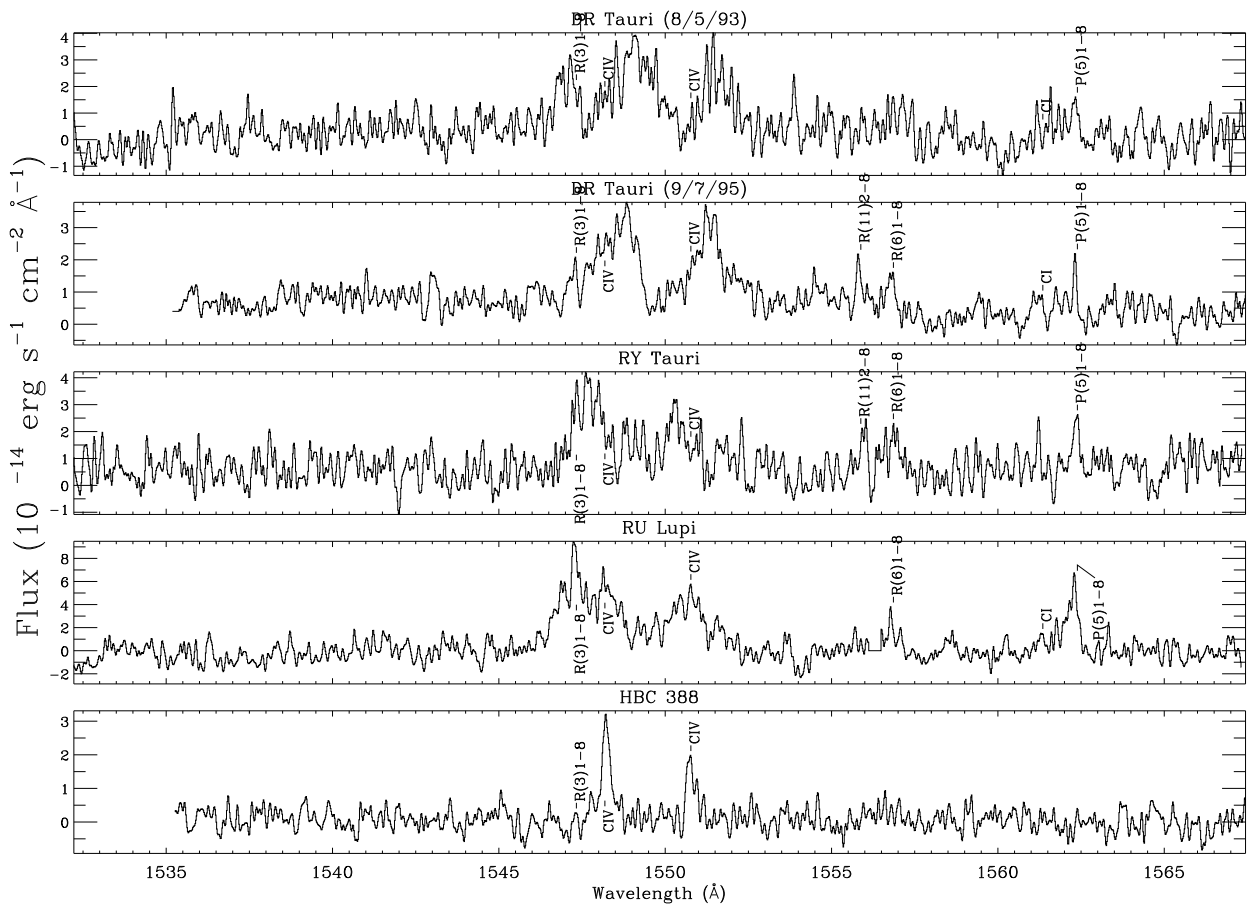


Fig. 6.— Smoothed spectra centered around 1550 Å, cont.

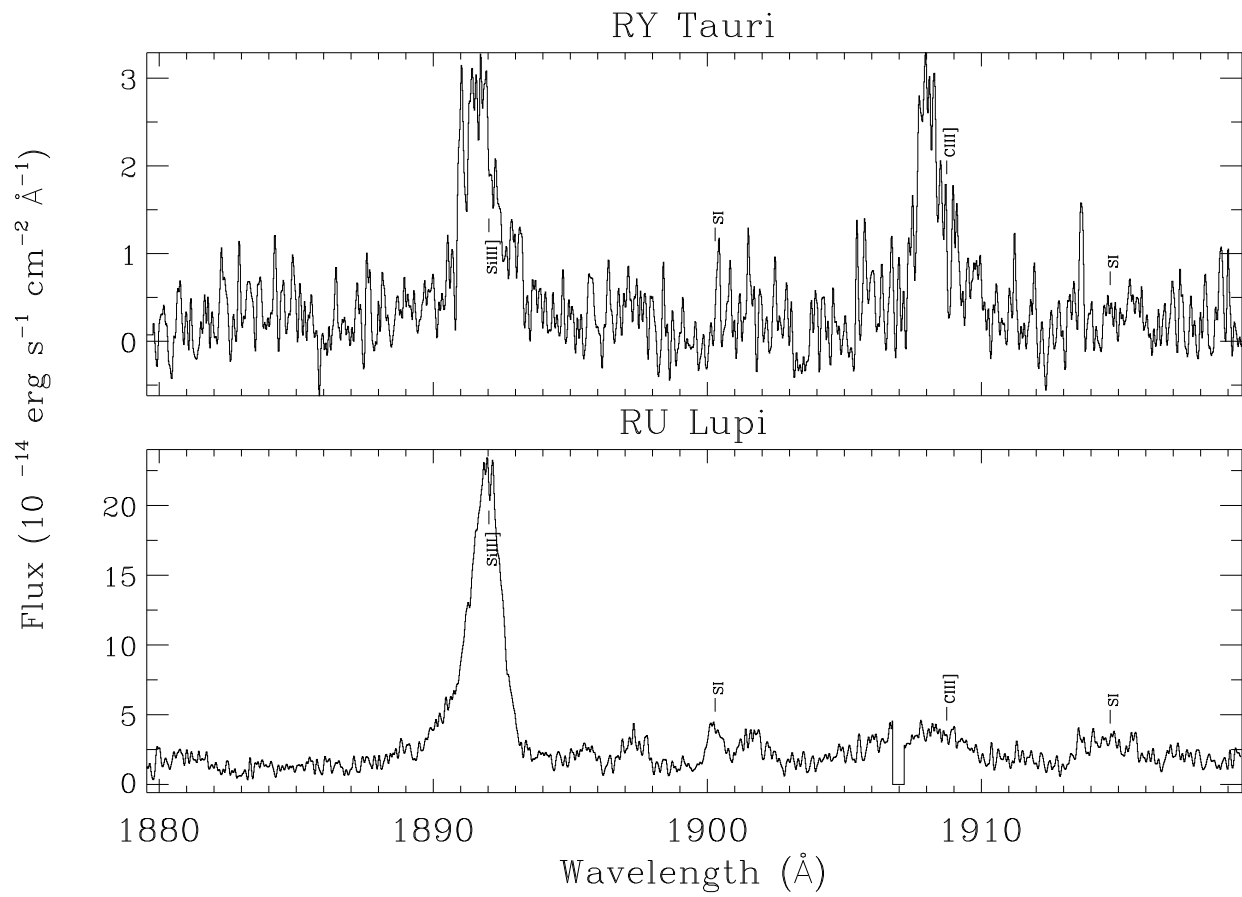


Fig. 7.— Smoothed spectra centered around 1900 Å.

have measured fluxes or upper limits in all the H₂ lines that are detected in at least one star. If a given line is not explicitly indicated it means that it was not in the spectral range observed for a given star. For those lines that are not detected we obtain 2- σ upper limits. These limits are obtained assuming a width equal to the average of all the other H₂ lines in the star, integrating a smoothed noise vector over the width, and multiplying by two. Such procedure produces upper-limits which coincide with those produced by more formal Montecarlo simulations. These limits are indicated in Table 3 without centroid velocity. Some of H₂ line fluxes were obtained by estimating their intensity from other lines in the same fluorescent route (Section 4.1). They are quoted in the Table without errors. In quoting the parameters for C IV and Si IV in Table 3, the H₂ emission has been subtracted from the profile, as discussed in section 4.3.

Table 2—Continued

Target Date	λ_{cen} (Å)	UT start (UT)	Exposure (sec.) (sec.)	Readouts	Root
9/7/95	1343.0	22:11:23	1408	5	Z2WB0209
HBC388	1552.9	11:25:49	5068	18	Z2WB0404
9/9/95	1401.0	15:59:47	5632	20	Z2WB0407
T Tau	1342.9	2: 9:34	1280	5	Z2WB0306
9/11/95	1497.3	3:21:58	1280	5	Z2WB0307
	1552.9	3:46:36	1126	4	Z2WB0308
	1401.0	4:57:32	2304	9	Z2WB030A
DG Tau	1552.6	2: 7:40	5068	18	Z2WB0106
2/8/96	1400.7	5:23:35	10418	37	Z2WB0109,B
	1400.7	8:35:22	5068	18	Z2WB010B

Table 3. Line Measurements

Line	Center ^a	FWHM ^b	Flux ^c	Unred. Flux ^c
BP Tauri				
R(0)0-5 (1393.72 Å)	...	60	< 0.6	< 2
P(2)0-5 (1398.95 Å)	-4 ± 7	50 ± 10	0.3 ± 0.1	1.2 ± 0.4
R(1)0-5 (1393.96 Å)	...	60	< 0.6	< 2
P(3)0-5 (1402.65 Å)	...	60	< 0.6	< 2
P(1)0-5 (1396.22 Å)	...	60	< 0.6	< 2
P(4)0-5 (1407.29 Å)	...	60	< 0.5	< 2
R(3)1-8 (1547.33 Å)	13 ± 9	60 ± 20	0.5 ± 0.2	1.7 ± 0.8
P(5)1-8 (1562.39 Å)	6 ± 6	70 ± 10	0.9 ± 0.2	3.1 ± 0.7
R(6)1-8 (1556.86 Å)	...	60	< 1	< 4
R(11)2-5 (1399.23 Å)	-11 ± 7	30 ± 20	0.3 ± 0.2	1.0 ± 0.6
R(11)2-8 (1555.88 Å)	...	60	< 1	< 4
SiIV (1393.755 Å) NC	-1.0 ± 5	100 ± 20	3.0 ± 0.5	11 ± 2
BC	5 ± 20	400 ± 100	3 ± 1	11 ± 5
SiIV (1402.770 Å) NC	5 ± 8	100 ± 30	1.3 ± 0.4	5 ± 2
BC	10 ± 30	340 ± 60	2.9 ± 0.9	11 ± 4
CIV (1548.187 Å) NC	11 ± 2	81 ± 4	4.3 ± 0.3	15 ± 1
BC	-10 ± 5	300 ± 10	11.7 ± 0.6	40 ± 2
CIV (1550.772 Å) NC	6 ± 3	80 ± 6	2.1 ± 0.3	7.1 ± 0.9
BC	-0 ± 6	300 ± 10	6.2 ± 0.4	21 ± 1
T Tauri				
R(0)0-4 (1333.47 Å)	-22 ± 7	30 ± 20	0.5 ± 0.2	50 ± 30
P(2)0-4 (1338.57 Å)	-20 ± 5	50 ± 10	1.0 ± 0.3	110 ± 30
R(0)0-5 (1393.72 Å)	-5	40	0.36	32.4
P(2)0-5 (1398.95 Å)	-5 ± 1	40 ± 2	0.73 ± 0.04	63 ± 3
R(1)0-4 (1333.80 Å)	-33 ± 4	50 ± 20	0.5 ± 0.2	60 ± 20
P(3)0-4 (1342.26 Å)	-21 ± 2	37 ± 5	1.0 ± 0.2	110 ± 20
R(1)0-5 (1393.96 Å)	-8	40	0.68	58.7
P(3)0-5 (1402.65 Å)	-8	40	0.96	82.2
P(1)0-5 (1396.22 Å)	...	50	< 0.5	< 50
P(4)0-4 (1346.91 Å)	...	50	< 0.5	< 50
P(4)0-5 (1407.29 Å)	...	50	< 0.5	< 40

Table 3—Continued

Line	Center ^a	FWHM ^b	Flux ^c	Unred. Flux ^c
R(3)1-7 (1489.56 Å)	-5 ± 4	70 ± 10	2.2 ± 0.5	140 ± 30
P(5)1-7 (1504.75 Å)	-9 ± 3	63 ± 7	2.4 ± 0.3	160 ± 20
R(3)1-8 (1547.33 Å)	-12	91	2.1	120
P(5)1-8 (1562.39 Å)	-3 ± 2	90 ± 3	2.1 ± 0.1	120 ± 6
R(6)1-7 (1500.44 Å)	-0.4 ± 7	80 ± 20	1.3 ± 0.4	80 ± 30
R(6)1-8 (1556.86 Å)	-14 ± 9	130 ± 20	1.8 ± 0.3	110 ± 20
P(13)2-3 (1325.34 Å)	...	50	< 0.5	< 60
R(11)2-5 (1399.23 Å)	...	50	< 0.6	< 50
R(11)2-8 (1555.88 Å)	-18 ± 2	24 ± 5	0.6 ± 0.2	36 ± 9
SiIV (1393.755 Å)	-15 ± 7	220 ± 20	3.6 ± 0.4	320 ± 30
SiIV (1402.770 Å)	-50 ± 10	220 ± 30	2.2 ± 0.4	190 ± 30
CIV (1548.187 Å)	-25 ± 6	250 ± 10	11.8 ± 0.9	700 ± 50
CIV (1550.772 Å)	0 ± 6	150 ± 10	4.8 ± 0.6	280 ± 40
DF Tauri				
R(0)0-4 (1333.47 Å)	-7 ± 8	60 ± 20	1.0 ± 0.3	3 ± 1
P(2)0-4 (1338.57 Å)	-6 ± 2	58 ± 4	1.3 ± 0.1	4.6 ± 0.4
R(0)0-5 (1393.72 Å)	...	30	< 0.4	< 1
P(2)0-5 (1398.95 Å)	-12 ± 4	70 ± 10	1.7 ± 0.3	6 ± 1
R(1)0-4 (1333.80 Å)	-5 ± 3	60 ± 10	1.8 ± 0.4	6 ± 1
P(3)0-4 (1342.26 Å)	-8 ± 2	62 ± 4	1.8 ± 0.1	6.1 ± 0.4
R(1)0-5 (1393.96 Å)	-18 ± 3	94 ± 6	3.8 ± 0.3	12 ± 1
P(3)0-5 (1402.65 Å)	-7 ± 3	89 ± 7	3.4 ± 0.3	11 ± 1
P(1)0-5 (1396.22 Å)	-14 ± 5	80 ± 10	1.4 ± 0.3	4 ± 1
P(4)0-4 (1346.91 Å)	-6 ± 5	30 ± 10	0.4 ± 0.2	1.3 ± 0.6
P(4)0-5 (1407.29 Å)	-8 ± 6	40 ± 10	0.8 ± 0.3	2.7 ± 1
R(3)1-8 (1547.33 Å)	...	30	< 0.5	< 2
P(5)1-8 (1562.39 Å)	5 ± 4	24 ± 8	0.4 ± 0.1	1.1 ± 0.4
R(6)1-8 (1556.86 Å)	...	30	< 0.4	< 1
R(11)2-5 (1399.23 Å)	-7 ± 5	30 ± 10	0.4 ± 0.2	1.2 ± 0.6
R(11)2-8 (1555.88 Å)	...	30	< 0.4	< 1
SiIV (1393.755 Å)	...	300	< 4	< 14
SiIV (1402.770 Å)	...	300	< 4	< 14
CIV (1548.187 Å) C1	10 ± 10	350 ± 30	10 ± 1	28 ± 4
C2	19.5 ± 0.9	41 ± 5	6.0 ± 0.5	18 ± 1
C3	42 ± 2	122 ± 4	17.7 ± 0.9	52 ± 3

Table 3—Continued

Line	Center ^a	FWHM ^b	Flux ^c	Unred. Flux ^c
CIV (1550.772 Å) C1	10 ± 10	320 ± 20	9 ± 1	25 ± 3
C2	18 ± 1	52 ± 3	5.3 ± 0.4	15 ± 1
C3	60 ± 20	130 ± 30	1.8 ± 0.6	5 ± 2
RW Auriga				
R(0)0-5 (1338.57 Å)	...	50	< 1	< 23
P(2)0-5 (1398.95 Å)	4 ± 3	80 ± 20	1.8 ± 0.7	40 ± 10
R(1)0-5 (1393.96 Å)	-20	60	1.4	28
P(3)0-5 (1402.65 Å)	-0 ± 2	49 ± 5	2.4 ± 0.3	47 ± 6
P(1)0-5 (1396.22 Å)	...	50	< 0.8	< 16
P(4)0-5 (1407.29 Å)	...	50	< 0.8	< 16
R(3)1-8 (1547.33 Å)	15.4	60	1.5	23
P(5)1-8 (1562.39 Å)	-6 ± 5	70 ± 10	1.4 ± 0.3	21 ± 5
R(6)1-8 (1556.86 Å)	...	50	< 1	< 15
R(11)2-5 (1399.23 Å)	5 ± 6	20 ± 20	< 0.6	< 12
R(11)2-8 (1555.88 Å)	...	50	< 1	< 15
SiIV (1393.755 Å)	160 ± 20	290 ± 30	19 ± 2	380 ± 40
SiIV (1402.770 Å)	-20 ± 8	500 ± 20	25 ± 2	490 ± 40
CIV (1548.187 Å) ^d	14 ± 5	220 ± 80
CIV (1550.772 Å) ^d	9 ± 4	140 ± 60
DG Tauri				
R(0)0-5 (1393.72 Å)	-4 ± 6	40 ± 10	0.4 ± 0.1	27 ± 9
P(2)0-5 (1398.95 Å)	-9 ± 2	39 ± 5	0.9 ± 0.1	59 ± 8
R(1)0-5 (1393.96 Å)	-4 ± 3	38 ± 6	0.9 ± 0.2	60 ± 10.
P(3)0-5 (1402.65 Å)	-10 ± 1	47 ± 3	1.5 ± 0.1	97 ± 9
P(1)0-5 (1396.22 Å)	-3 ± 5	60 ± 20	0.3 ± 0.1	19 ± 7
P(4)0-5 (1407.29 Å)	-20 ± 10.	40 ± 30	< 0.4	< 40
R(3)1-8 (1547.33 Å)	0.0	27.3	0.32	15.0
P(5)1-8 (1562.39 Å)	-12 ± 2	24 ± 6	0.3 ± 0.1	14 ± 5
R(6)1-8 (1556.86 Å)	-7 ± 6	30 ± 10	0.2 ± 0.1	10 ± 7
R(11)2-5 (1399.23 Å)	-9 ± 5	40 ± 10	0.4 ± 0.1	27 ± 9
R(11)2-8 (1555.88 Å)	-4 ± 3	42 ± 7	0.6 ± 0.1	28 ± 6

Table 3—Continued

Line	Center ^a	FWHM ^b	Flux ^c	Unred. Flux ^c
SiIV (1393.755 Å)	...	200	< 1.3	< 80
SiIV (1402.770 Å)	...	200	< 1.3	< 80
CIV (1548.187 Å)	-260 ± 6	170 ± 10	2.7 ± 0.3	140 ± 20
CIV (1550.772 Å)	-270 ± 10	230 ± 30	1.7 ± 0.3	90 ± 20
DR Tauri (8/5/93)				
R(0)0-4 (1333.47 Å)	...	40	< 0.4	< 10
P(2)0-4 (1338.57 Å)	...	40	< 0.3	< 7
R(0)0-5 (1393.72 Å)	...	40	< 0.4	< 10
P(2)0-5 (1398.95 Å)	...	40	< 0.3	< 8
R(1)0-4 (1333.80 Å)	...	40	< 0.4	< 10
P(3)0-4 (1342.26 Å)	-11 ± 3	45 ± 7	0.36 ± 0.07	10 ± 2
R(1)0-5 (1393.96 Å)	-15 ± 6	50 ± 20	0.6 ± 0.3	14 ± 7
P(3)0-5 (1402.65 Å)	-4 ± 2	30 ± 5	0.6 ± 0.1	13 ± 3
P(1)0-5 (1396.22 Å)	...	40	< 0.4	< 10
P(4)0-4 (1346.91 Å)	...	40	< 0.3	< 8
P(4)0-5 (1407.29 Å)	...	40	< 0.4	< 8
R(3)1-8 (1547.33 Å)	-15	40	0.3	5.3
P(5)1-8 (1562.39 Å)	-15 ± 7	50 ± 20	0.4 ± 0.2	8 ± 4
R(6)1-8 (1556.86 Å)	...	40	< 0.5	< 9
R(11)2-5 (1399.23 Å)	...	40	< 0.4	< 9
R(11)2-8 (1555.88 Å)	...	40	< 0.5	< 8
SiIV (1393.755 Å)	...	150	< 1.5	< 40
SiIV (1402.770 Å)	...	150	< 1.5	< 40
CIV (1548.187 Å) C1	-250 ± 10	90 ± 20	0.9 ± 0.3	16 ± 5
C2	130 ± 10	150 ± 20	$2.0 \pm .2$	40 ± 4
CIV (1550.772 Å) C1	-260 ± 20	90 ± 20	1 ± 1	20 ± 20
C2	147 ± 9	150 ± 20	1.8 ± 0.4	31 ± 6
DR Tauri (9/7/95)				
R(0)0-4 (1333.47 Å)	...	20	< 0.1	< 3
P(2)0-4 (1338.57 Å)	-19 ± 5	50 ± 10	0.3 ± 0.1	9 ± 3
R(1)0-4 (1333.80 Å)	...	20	< 0.1	< 2
P(3)0-4 (1342.26 Å)	-3 ± 3	20 ± 2	0.25 ± 0.07	7 ± 2
P(4)0-4 (1346.91 Å)	...	20	< 0.1	< 3

Table 3—Continued

Line	Center ^a	FWHM ^b	Flux ^c	Unred. Flux ^c
R(3)1-8 (1547.33 Å)	–14	20	0.25	0.43
P(5)1-8 (1562.39 Å)	–14 ± 2	14 ± 4	0.21 ± 0.05	3.7 ± 0.9
R(6)1-8 (1556.86 Å)	–5 ± 4	29 ± 8	0.19 ± 0.07	3 ± 1
R(11)2-8 (1555.88 Å)	–13 ± 2	26 ± 5	0.21 ± 0.05	3.7 ± 0.9
CIV (1548.187 Å)	75 ± 6	240 ± 20	3.3 ± 0.3	59 ± 5
CIV (1550.772 Å)	110 ± 6	190 ± 10	2.4 ± 0.2	42 ± 4
RY Tauri				
R(0)0-5 (1393.72 Å)	...	50	< 0.6	< 1.3
P(2)0-5 (1398.95 Å)	9 ± 4	48 ± 8	0.7 ± 0.2	1.5 ± 0.4
R(1)0-5 (1393.96 Å)	2 ± 5	20 ± 20	< 0.6	< 1.3
P(3)0-5 (1402.65 Å)	–2 ± 6	60 ± 20	1.0 ± 0.3	2.1 ± 0.6
P(4)0-5 (1407.29 Å)	...	50	< 0.6	< 1.3
P(1)0-5 (1396.22 Å)	...	50	< 0.6	< 1.3
R(3)1-8 (1547.33 Å)	–4	50	0.47	2.95
P(5)1-8 (1562.39 Å)	–8 ± 4	44 ± 8	0.5 ± 0.1	1.0 ± 0.2
R(6)1-8 (1556.86 Å)	...	50	< 0.6	< 1.2
R(11)2-5 (1399.23 Å)	...	50	< 0.6	< 1.3
R(11)2-8 (1555.88 Å)	...	50	< 0.6	< 1.2
SiIV (1393.755 Å)	...	150	< 2	< 4.3
SiIV (1402.770 Å)	...	150	< 2	< 4.3
CIV (1548.187 Å)	78 ± 8	160 ± 20	2.7 ± 0.4	5.4 ± 0.8
CIV (1550.772 Å)	80 ± 10	140 ± 20	1.5 ± 0.3	3.0 ± 0.6
RU Lupi				
R(0)0-5 (1393.72 Å)	...	40	< 0.7	< 20
P(2)0-5 (1398.95 Å)	–4 ± 7	30 ± 20	0.4 ± 0.4	10 ± 10
R(1)0-5 (1393.96 Å)	–12	30	0.37	10.7
P(3)0-5 (1402.65 Å)	–12	30	0.51	14.7
P(1)0-5 (1396.22 Å)	...	40	< 0.5	< 20
P(4)0-5 (1407.29 Å)	...	40	< 0.6	< 20

4.1. Molecular hydrogen

The spectra show a large number of H_2 lines. These correspond to transitions in the Lyman Band of molecular hydrogen, $B^1\Sigma_u^+$ to $X^1\Sigma_g^+$. In this work we use the H_2 parameters derived by Abgrall et al. (1993). Table 3 shows the measured parameters of all the lines present in at least one spectrum. Each transition is indicated in standard notation: the letter tells the change in rotational level from the upper to the lower level ($J''-J'=1$ is P, $J''-J'=-1$ is R), the number in parenthesis indicates the J'' value (the rotational level of the lower energy state), and the two final numbers indicate the vibrational levels v' , v'' of the upper and lower levels, respectively, for the transition. Table 3 also shows the upper limits of the lines that are not observed in a given star. We have made no attempt to obtain unblended fluxes for the H_2 lines near C II (1335 Å).

Table 4 summarizes the H_2 lines detected in each star. For optically thin lines the ratio of the flux values of two lines with the same upper level should be given by the ratio of the A-values to the wavelength of the transition. For almost every star (except DF Tau, see below) that shows at least two lines with the same upper level, this is the case. This leads us to conclude that H_2 levels with $v'' \geq 4$ are optically thin.

The validity of this conclusion depends on the assumption that reddening from Table 1 are valid, and that the extinction is the same for the ultraviolet H_2 emission lines and for the optical spectra (from which A_V is determined). Given the S/N of the spectra, the flux ratios used here are not very sensitive to errors in the absolute (and poorly determined) extinction values, as observed lines of the same route are generally less than a 1000 Å from each other. For this same reason, it is difficult to estimate whether or not there is differential extinction between the star and the region responsible for the H_2 emission.

By using other lines in the same fluorescent route we can obtain estimates of the intensities of the lines blended with C IV (R(3)1-8) and Si IV (R(0)0-5, R(1)0-5, and P(3)0-5). The procedure is outlined in detail for some stars in section 4.2. Also indicated in Table 4 is the average FWHM and the average shift in velocity for all the H_2 lines in each star.

In DF tau, the ratios within the fluxes of the four lines belonging to the upper level $v'=2$, $J'=0$, do not follow the values expected for optically thin emission. R(0)0-5 and P(3)0-5 coincide with the positions of the Si IV resonance doublet, and we have obtained their fluxes assuming that all the observed emission is H_2 . From the appearance of the spectra, this is a reasonable assumption, but the fact that we do not obtain ratios consistent with optically thin emission may be telling us that there is indeed some underlying Si IV emission. Roughly half of the flux in R(0)0-5 and P(3)0-5 would have to be Si IV to make their fluxes have a value consistent with optically thin emission. The two lines also have

Table 3—Continued

Line	Center ^a	FWHM ^b	Flux ^c	Unred. Flux ^c
R(3)1-8 (1547.33 Å)	–17	40	2.0	42
P(5)1-8 (1562.39 Å)	–28 ± 4	78 ± 8	2.3 ± 0.3	50 ± 6
R(6)1-8 (1556.86 Å)	–16 ± 3	16 ± 6	0.3 ± 0.1	7 ± 3
R(11)2-5 (1399.23 Å)	...	40	< 0.5	< 10
R(11)2-8 (1555.88 Å)	...	40	< 0.8	< 20
SiIV (1393.755 Å)	5 ± 5	270 ± 10	10.8 ± 0.7	310 ± 20
SiIV (1402.770 Å)	–31 ± 6	250 ± 10	8.5 ± 0.6	240 ± 20
CIV (1548.187 Å)	–20 ± 20	340 ± 40	8 ± 1	170 ± 20
CIV (1550.772 Å)	–10 ± 10	300 ± 30	6.6 ± 0.8	140 ± 20
HBC 388				
R(0)0-5 (1393.72 Å)	...	40	< 0.2	< 0.2
P(2)0-5 (1398.95 Å)	...	40	< 0.2	< 0.2
R(1)0-5 (1393.96 Å)	...	40	< 0.2	< 0.2
P(3)0-5 (1402.65 Å)	...	40	< 0.2	< 0.2
P(1)0-5 (1396.22 Å)	...	40	< 0.2	< 0.2
P(4)0-5 (1407.29 Å)	...	40	< 0.2	< 0.2
R(3)1-8 (1547.33 Å)	...	40	< 0.3	< 0.3
P(5)1-8 (1562.39 Å)	...	40	< 0.3	< 0.3
R(6)1-8 (1556.86 Å)	...	40	< 0.3	< 0.3
R(11)2-5 (1399.23 Å)	...	40	< 0.2	< 0.2
R(11)2-8 (1555.88 Å)	...	40	< 0.2	< 0.3
SiIV (1393.755 Å)	–1 ± 7	130 ± 20	0.7 ± 0.1	0.9 ± 0.2
SiIV (1402.770 Å)	0 ± 10	110 ± 30	0.4 ± 0.1	0.5 ± 0.1
CIV (1548.187 Å)	8 ± 3	61 ± 7	0.9 ± 0.2	1.2 ± 0.2
CIV (1550.772 Å)	–0 ± 4	52 ± 9	0.5 ± 0.1	0.6 ± 0.1

Note. — All wavelengths are in the stellar rest frame. The errors in each measurement are indicated. For measurements without errors, the parameters of the fit have been assumed from neighboring lines. The upper limits (2σ) of the H₂ lines have been obtained by integrating a smooth noise vector (multiplied by 2) over the indicated FWHM, which corresponds to the average of other H₂ lines. “NC” stands for narrow component, “BC” is broad component. In DF Tau, we decompose CIV in three components labeled C1, C2, and C3.

^aUnits are km s^{–1}.

^bUnits are km s^{–1}.

^cUnits are 10^{–14} ergs sec^{–1} cm^{–2}.

^dMeasured directly over the spectrum (i.e., without a Gaussian fit).

Table 4. H_2 Lines Observed

Line	BP Tau	T Tau	DF Tau	RW Aur	DG Tau	DR Tau (8/5/93)	DR Tau (9/7/95)	RY Tau	RU Lup
Average shift (km s^{-1})	0 ± 3	-9.7 ± 0.7	-2.2 ± 0.5	0.5 ± 2	-9.2 ± 0.9	-7 ± 2	-11 ± 1	0 ± 2	-18 ± 2
Average FWHM (km s^{-1})	57 ± 8	52 ± 2	27.4 ± 0.8	52 ± 4	41 ± 2	36 ± 4	20 ± 2	46 ± 5	37 ± 5
R(0)0-4 (1333.47 Å)	...	y	y	u	u
P(2)0-4 (1338.57 Å)	...	y	y	u	y
R(0)0-5 (1393.72 Å)	u	s	u	s	y	u	u	u	u
P(2)0-5 (1398.95 Å)	y	y	y	y	y	u	...	y	y
R(1)0-4 (1333.80 Å)	...	y	y	u	u
P(3)0-4 (1342.26 Å)	...	y	y	y	y
R(1)0-5 (1393.96 Å)	u	s	y	s	y	y	...	y	s
P(3)0-5 (1402.65 Å)	u	s	y	y	y	y	...	y	s
P(1)0-5 (1396.22 Å)	u	u	y	u	y	u	...	u	u
P(4)0-4 (1346.91 Å)	...	u	y	u	u
P(4)0-5 (1407.29 Å)	u	u	y	u	u	u	u	u	u
R(3)1-7 (1489.56 Å)	...	y
P(5)1-7 (1504.75 Å)	...	y
R(3)1-8 (1547.33 Å)	y	s	u	s	s	s	s	s	s
P(5)1-8 (1562.39 Å)	y	y	y	y	y	y	y	y	y
R(6)1-7 (1500.44 Å)	...	y
R(6)1-8 (1556.86 Å)	u	u	u	u	y	u	y	u	y
R(11)2-5 (1399.23 Å)	y	u	y	y	y	u	...	u	u
R(11)2-8 (1555.88 Å)	u	y	u	u	y	u	y	u	u

Note. — The letters mean the following: u: upper limit (This is a 2σ limit), y: parameters measured (by fitting a Gaussian to the line), s: parameters estimated (by using other lines from the same fluorescent route). Three dots indicate that the spectral range in which the line is present is not available.

some of the largest FWHM measured for H₂. These two facts suggest that the core of a broad Si IV line is affecting the measurement of H₂. Given the quality of our spectra, we choose not to explore this issue further (but see section 4.3).

We do not detect any significant systematic change in the FWHM of the lines with wavelength. There are no correlations between FWHM and velocity shift (either average quantities or individual lines), or between FWHM, velocity shift, and the inclination of the star. Notice, however, that the average of the line shifts is always less or equal to zero. Here we should remember that systematic errors in the velocity (up to 20 km s⁻¹) may appear due to inaccurate centering of the star in the slit. This means that velocity shifts from star to star cannot be compared. However, random centering errors should produce random positive and negative shifts. The fact that the H₂ lines are blueshifted (in average) may indicate that they are formed in material moving towards the observer.

The resolving power of the GHRS instrument at 1500 Å is \sim 15 km s⁻¹. The widths of the H₂ emission are larger than this, due either to turbulence or to a partially filled aperture. As noted in the introduction, extended H₂ emission is indeed detected in T Tauri stars. A uniformly filled aperture would produce a flat-topped profile with a base width larger than 100 km s⁻¹. Non-uniformly filled apertures will produce sharper, narrower lines. We do not observe flat-topped profiles, and all the detected lines have a single clear peak. Errico et al. (2000) claim (using these same data) that a double peaked profile is present in the P(5)1-8 line (1562.39 Å) of RW Aur. However, this is a region with very poor signal-to-noise, which leads us to conclude that the double peaked profile is not significant. The similarity of the average widths of the H₂ lines for all stars suggests that the emission is extended in all, although its angular scale is likely to be less than 2 arcsecs.

These H₂ lines are thought to be due to fluorescence, excited by strong atomic lines. In the Sun, H_{Lyα}, Si IV, and C IV, have been identified, among others, as the sources of the excitation (Jordan et al. 1978; Bartoe et al. 1979). This conclusion is reached by using the observed strength of the H_{Lyα} line and predicting what is the strength of the H₂ excitation produced. Insight into the nature of the exciting process can be obtained by calculating the populations of the levels from which the fluorescent routes are excited.

Observations of the H_{Lyα} line for TTS have been performed by the IUE satellite. As reported by Blondel, Talavera, & Djie (1993), four observations of the H_{Lyα} region are available in the IUE database. These correspond to TW Hya, RU Lup, DR Tau, and T Tau (only upper limits are derived for the last two). The spectra show a redshifted emission peak in the location of the H_{Lyα} line. Kurt & Lamzin (1995) argue that the blue wing of the line should be strongly affected by ISM absorption. In addition, H_{Lyα} is expected to show a strong wind signature that will absorb emission in the blue wing. This is the case in the

STIS spectrum of TW Hya analyzed by Herczeg et al. (2001).

If we assume that the $H_{Ly\alpha}$ line can be described by a Gaussian, then for RU Lup, $F_p = 2 \times 10^{-13}$ ergs sec $^{-1}$ cm $^{-2}$ Å, $\sigma = 2.01$ Å, where F_p is the peak flux, uncorrected for extinction, and σ is the Gaussian line width). For the reasons mentioned above, the total flux (corrected by ISM and wind absorption) is probably 3-4 times larger. As Table 3 show, these fluxes are larger than the fluxes in the Si IV and C IV lines, which are of the order of 10^{-14} ergs sec $^{-1}$ cm $^{-2}$ Å (without taking the extinction into account). In the particular case of RU Lup, the $H_{Ly\alpha}$ flux is 34 times larger than the flux in the blue member of the C IV doublet. In what follows we therefore assume that fluorescence by other atomic species is negligible compared to the fluorescence by $H_{Ly\alpha}$ (and perhaps other lines of the Lyman series).

Another possible pumping source for H_2 is the strong UV continuum of TTS. If the UV continuum were an important source of photons for the excitation of H_2 we would see fluorescent lines coming from a wide range of wavelengths. However, as Figure 8 shows, all the observed lines are excited within a few Ångstroms of $H_{Ly\alpha}$. Furthermore, for TW Hya Herczeg et al. (2001) show that the continuum is three orders of magnitude weaker than the $H_{Ly\alpha}$ peak flux. Therefore, $H_{Ly\alpha}$ dominates the fluorescence process. All of the fluorescent routes we observe have a strong line within 4 Å (~ 1000 km s $^{-1}$) of the center of $H_{Ly\alpha}$ (Figure 8).

To understand the physical conditions of the region producing the emission, we need to know about the strength and angular coverage of the exciting agent (assumed here to be $H_{Ly\alpha}$) at the exciting wavelength in the spatial position where the excitation takes place, and the population of the state that will be excited. However, the fluorescent process produces only one observed quantity: the population of the upper level from which fluorescence takes place. Many lines are observed from a given fluorescent route, but, if optically thin, they all measure the same quantity: the population of the upper level from which they come. Even if we knew exactly where the H_2 is in relation to the star, what fraction of the star emits the $H_{Ly\alpha}$ radiation responsible for the excitation, and what fraction is intercepted by the H_2 , we would still have a mathematical problem with n equations (the number of fluorescent routes observed) and $2n$ unknowns (for each fluorescent route, the population of the exciting state and the strength of $H_{Ly\alpha}$ at the excitation wavelength).

To solve this degeneracy, assumptions must be made, either about the population distribution of H_2 or the shape of the $H_{Ly\alpha}$ line. In what follows, we assume that we know the shape and strength of the $H_{Ly\alpha}$ line, and obtain the column densities of the exciting H_2 states. We will show that such a procedure requires non-thermal populations. An alternative procedure would be to assume a certain distribution of the levels of H_2 and from the

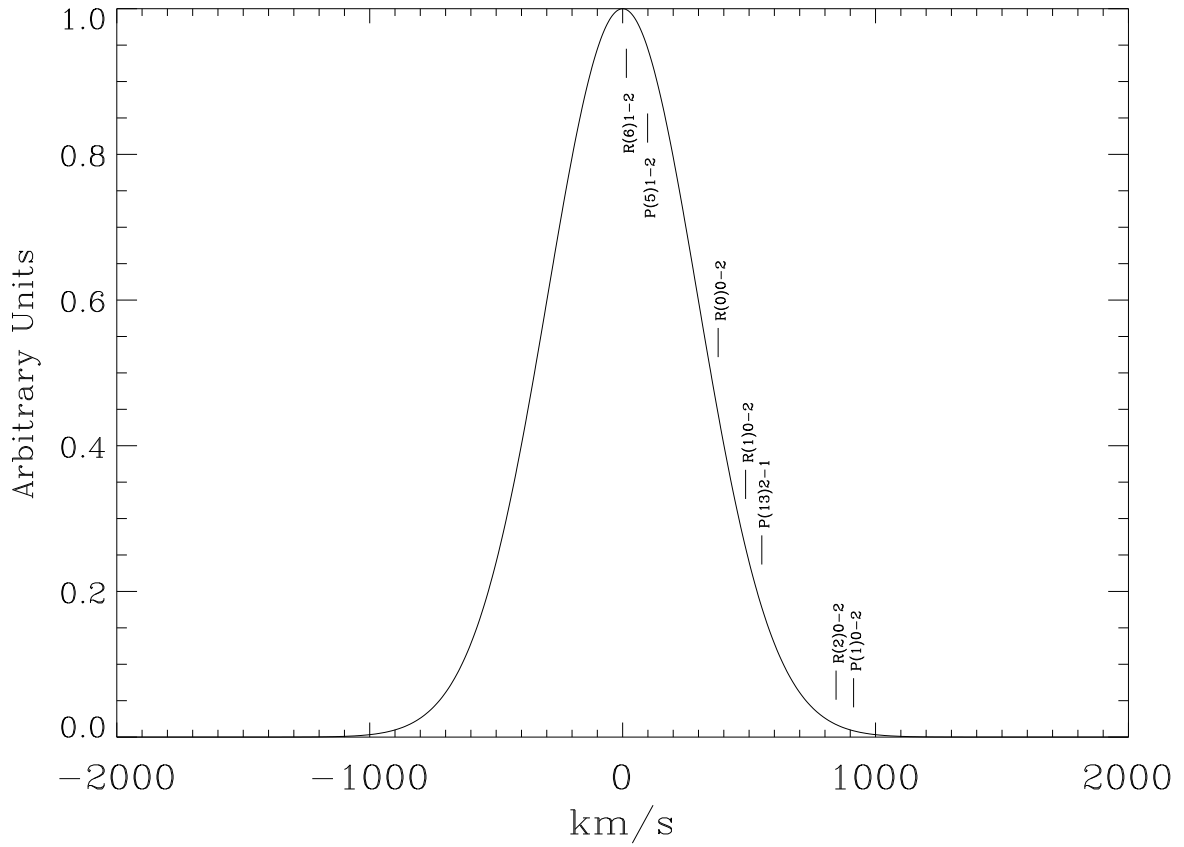


Fig. 8.— Example of a Gaussian $H_{Ly\alpha}$ line with $\text{FWHM}=680 \text{ km s}^{-1}$ (or $\sigma=1.2 \text{ \AA}$). Indicated are the transitions from which fluorescence is observed in at least one star in our spectra. The line $P(1)0-2$ is at $1219.37, 912.4 \text{ km s}^{-1}$ to the red of the $H_{Ly\alpha}$ peak.

observed lines reconstruct the $H_{Ly\alpha}$ profile. We do not have enough observed routes to carry on this procedure (the maximum number of routes observed in a given star is six).

4.1.1. A Gaussian Shape for $H_{Ly\alpha}$

The flux in an H_2 line is given by:

$$F_{ul} = \frac{A_{sp}}{4\pi d^2} \frac{hc}{\lambda_{ul}} N_u A_{ul} \quad (1)$$

where F_{ul} is the integrated flux of the observed line (corrected for extinction), A_{sp} is the fraction of the spectrograph aperture from which the emission comes, d is the distance to the star, h and c are the Planck constant and the speed of light, respectively, N_u is the column density of H_2 in the upper level, and A_{ul} is the Einstein A-value of the transition. In the statistical equilibrium equation

$$N_u \sum_{\sigma} A_{u\sigma} = \sum_s N_s B_{su} J_{\nu} \quad (2)$$

we neglect stimulated emission and collisions among upper levels. The term on the right represents the absorption of $H_{Ly\alpha}$ photons (B_{su} is the Einstein B-coefficient, J_{ν} is the mean specific intensity in the position where the absorption occurs). From this we obtain (McMurtry, Jordan, & Carpenter 1999):

$$F_{ul} = \beta \frac{1}{4\pi} \sum_s \frac{g_u}{g_s} \frac{\lambda_{us}^3}{\lambda_{ul}} \frac{A_{ul} A_{us}}{\sum_{\sigma} A_{u\sigma}} n_s \frac{\lambda_{Ly\alpha}}{\nu_{Ly\alpha}} F_{\lambda_{us}} \text{ ergs cm}^{-2} \text{ s}^{-1} \quad (3)$$

where g_u is the multiplicity of the upper level of the observed line, $\sum_{\sigma} A_{u\sigma}$ is the sum over the A-values of all the transitions from the same upper level. The sum on the left is over all the exciting transitions which contribute to a given upper level: g_s is the multiplicity of the level from which the line is excited, λ_{us} is the wavelength of the exciting transition, A_{us} is the A-value of the exciting transition, N_s is the column density of the H_2 molecules in the state from which fluorescence takes place, and $F_{\lambda_{us}}$ is the flux (in units of $\text{ergs sec}^{-1} \text{ cm}^{-2} \text{ \AA}$) from the exciting transition. This is the $H_{Ly\alpha}$ flux integrated over the H_2 line profile, which we assume is very sharp compared to the width of $H_{Ly\alpha}$ and therefore it can be approximated by a delta function. $\frac{\lambda_{Ly\alpha}}{\nu_{Ly\alpha}}$ converts the flux in per \AA to flux per Hz. Additionally, $\beta = \frac{A_{sp}}{8\pi d_*^2}$, where d_* is the distance from the source of $H_{Ly\alpha}$ to the position where the excitation takes

place. In what follows, we assume $\beta = 1$. In the absence of detailed information about the spatial distribution of H_2 this is a reasonable assumption.

From Equation 3 (with $\beta = 1$ and assuming the high temperature ortho/para ratio of 3:1 for H_2) we obtain the column density of the levels from which the exciting transition takes place (Table 5, in order of excitation energy from the ground state). For this Table we have assumed that the integrated flux in $\text{H}_{Ly\alpha}$ is 30 times larger than the blue C IV line flux (for RU Lup is 34 times larger), and that the $\text{H}_{Ly\alpha}$ emission is Gaussian with $\sigma \sim 1.2 \text{ \AA}$ (the value measured for TW Hya). To calculate the population of a given level we use the best determined fluorescent line (highest signal-to-noise) from the route excited from that level. Furthermore, we assume that the excitation is due to the energy of the exciting line closest to $\text{H}_{Ly\alpha}$. For the values of σ we are considering here this is an excellent assumption. The errors in the populations indicated in the Table have been obtained by propagating only the errors in the measured H_2 lines. They do not include errors in the $\text{H}_{Ly\alpha}$ flux and in the width of the line, which are impossible to determine with the IUE data and should dominate this kind of calculation. Errors of up to half a magnitude in the extinction estimates will produce variations in the densities consistent with the calculated random error.

The populations are weakly correlated between the stars. This is an indication that the characteristics of the $\text{H}_{Ly\alpha}$ emission dominate over differences in the temperature and density in the H_2 gas between different stars (Section 4.3.2).

The order of magnitude of the column densities indicates that the populations of the levels should not be thermal. The critical density for quadrupole transitions between the v'' levels is $\sim 10^6 \text{ cm}^{-3}$ (using the collisional cross sections from Martin & Mandy 1995). For an emission region $1 R_\odot$ thick, a 10^{14} cm^{-2} column density corresponds to a density of 10^3 cm^{-3} . Therefore, the density is very subcritical and radiative effects should be considered when calculating the equilibrium populations.

This point is made clear when we take the ratios of the populations in Table 5. The ratios are better determined than the populations themselves, as they do not suffer from the uncertainty in the $\text{H}_{Ly\alpha}$ intensity. In the Table we have indicated the value of the multiplicities (g'') of each level. This is expected to be the ratio of the populations at very high temperatures and very large σ s. In any other circumstance, the ratio of the population of a state with higher excitation energy to a state with lower excitation energy will be less than this value, if the populations are in LTE. As the Table shows, population inversions are present in most stars. This means that excitation temperatures derived from the ultraviolet H_2 lines do not correspond to the kinetic temperature of the emitting region, and the excitation cannot be explained by any process that produces a thermal distribution (like a shock). This point is made explicitly in Figure 9, in which we plot the level populations

Table 5. Derived Parameters for Pumped H₂ Levels

Line (v", J", g")	BP Tau	T Tau	DF Tau	RW Aur	DG Tau	DR Tau (8/5/93)	DR Tau (9/7/95)	RY Tau	RU Lup
$v''=2, J''=0, g''=1$									
$v=378.4 \text{ km s}^{-1}$									
τ	0.06 ± 0.02	0.30 ± 0.01	0.25 ± 0.02	0.5 ± 0.1	1.7 ± 0.2	...	1.1 ± 0.3	0.8 ± 0.2	0.3 ± 0.2
$N (10^{14} \text{ cm}^{-2})$	0.09 ± 0.03	0.35 ± 0.01	0.18 ± 0.02	0.7 ± 0.2	1.7 ± 0.2	...	0.5 ± 0.2	1.0 ± 0.3	0.3 ± 0.2
ratio	1	1	1	1	1	...	1	1	1
$v''=2, J''=1, g''=9$									
$v=486.5 \text{ km s}^{-1}$									
τ	...	0.8 ± 0.1	0.52 ± 0.03	1.2 ± 0.2	5.4 ± 0.5	1.9 ± 0.4	1.5 ± 0.4	2.2 ± 0.6	...
$N (10^{14} \text{ cm}^{-2})$...	13 ± 2	5.2 ± 0.3	22 ± 3	73 ± 7	25 ± 6	10 ± 3	40 ± 10	...
ratio	...	38 ± 7	28 ± 3	30 ± 10	43 ± 7	1 ^a	19 ± 8	40 ± 10	...
$v''=2, J''=2, g''=5$									
$v=843.1 \text{ km s}^{-1}$									
τ	4 ± 2
$N (10^{14} \text{ cm}^{-2})$	5 ± 2
ratio	30 ± 10
$v''=2, J''=5, g''=33$									
$v=98.5 \text{ km s}^{-1}$									
τ	0.16 ± 0.04	0.50 ± 0.02	0.06 ± 0.02	0.30 ± 0.07	0.6 ± 0.3	0.4 ± 0.2	0.5 ± 0.1	0.6 ± 0.1	1.3 ± 0.2
$N (10^{14} \text{ cm}^{-2})$	3.2 ± 0.7	9.0 ± 0.3	0.7 ± 0.2	6 ± 1	6 ± 2	8 ± 4	3.6 ± 0.9	9 ± 2	17 ± 2
ratio	40 ± 1	27 ± 2	3 ± 1	7 ± 3	3 ± 1	0.3 ± 0.2	7 ± 3	9 ± 3	50 ± 40
$v''=2, J''=6, g''=13$									
$v=13.9 \text{ km s}^{-1}$									
τ	...	0.44 ± 0.06	0.3 ± 0.2	...	0.4 ± 0.2	...	0.17 ± 0.07
$N (10^{14} \text{ cm}^{-2})$...	0.7 ± 0.1	0.4 ± 0.2	...	0.3 ± 0.1	...	0.21 ± 0.09
ratio	...	2.0 ± 0.4	0.2 ± 0.1	...	0.5 ± 0.2	...	0.7 ± 0.6
$v''=1, J''=13, g''=81$									
$v=550.9 \text{ km s}^{-1}$									
τ	0.3 ± 0.2	0.8 ± 0.2	0.4 ± 0.2	...	4 ± 1	...	2.6 ± 0.6
$N (10^{14} \text{ cm}^{-2})$	10 ± 6	25 ± 4	7 ± 3	...	80 ± 20	...	26 ± 6
ratio	110 ± 80	60 ± 20	40 ± 20	...	50 ± 10	...	50 ± 20

Note. — For each star we indicate the values derived for the exciting transition. For each exciting transition we give v'' and J'' , the vibrational and rotational numbers of the level from which the transition is excited. We also give the velocity of the transition with respect to the center of the H_{Lyα} line, the optical depth (τ) of the exciting line, the column density in units of 10^{14} cm^{-2} , and the ratio of the column density to that of level $N(v''=2, J''=0)$.

^aAs we do not have a measured column density of $N(v''=2, J''=0)$ for DR Tau (8/5/93) the ratios are given with respect to $N(v''=2, J''=1)$

divided by the multiplicity of the level, versus the energy of the level, for some of our stars. If the populations were thermal, all the points for each star should lie on a straight line (whose intercept with the ordinate axis is the total H_2 density), and they do not. Also indicated are the lines produced by a 1500 K distribution, with a total H_2 column density of $2 \times 10^{18} \text{ cm}^{-2}$. These are the parameters found by van den Ancker et al. (1999) for T Tau. While the solid line occupies the same general area as the observed distributions, it does not reproduce the observations. Errors in the assumed peak of the $H_{Ly\alpha}$ line make the mean value of the populations uncertain but do not change their relative values.

Based on the densities and the A-values, we calculate the optical depth of the pumped transition. Notice that the optical depths are less than one for most stars. The effect of a high optical depth is to effectively remove the line from the fluorescent cascade, as photons re-emitted in this wavelength will be absorbed very rapidly. This tends to equalize the flux in other lines from the same route. The ratios of the observed lines indicate that they are optically thin, which confirms our optical depth estimates.

The calculations in which Table 5 is based assume that the $H_{Ly\alpha}$ profile can be correctly modeled by a Gaussian. If the line shows self-reversals in the core, such assumption is false, and the populations of $N(v''=2, J''=6)$ and perhaps $N(v''=2, J''=5)$ are incorrect. The populations of $N(v''=2, J''=6)$ are consistently smaller than the populations of $N(v''=2, J''=5)$, in spite of the small energy difference between them. A NLTE self-reversal in $H_{Ly\alpha}$ that affected $N(v''=2, J''=6)$ more than $N(v''=2, J''=5)$ may make the populations more alike. It is unlikely that the core self-reversal is as large as to affect the other populations, which are excited at velocities larger than 300 km s^{-1} . More fundamentally, the $H_{Ly\alpha}$ line is more likely to resemble a Voigt profile. This will also change the core/wing ratios. We may be seeing some evidence of non-Gaussian wings. Two routes are excited from the $v''=2, J''=1$ level: one to level $v'=0, J'=0$ (excited at 900 km s^{-1} from the center of $H_{Ly\alpha}$) and the other to level $v'=0, J'=2$ (excited at 500 km s^{-1}). We observe the first route only in DF Tau and DG Tau, as the line P(1)0-5 at 1396 \AA . The first route predicts much larger densities (a factor of 30 and 7 for each star respectively) than the second, for the $v''=2, J''=1$ level. Assuming a Voigt profile with an a parameter of 0.2 will solve the discrepancy for DG Tau. For DF Tau a fairly large parameter is needed. However, while the densities of individual states change upon using a Voigt function, they are still not in thermal equilibrium. In Table 5 we use R(1)0-2, 500 km s^{-1} from the $H_{Ly\alpha}$ center, to calculate populations for $N(v''=2, J''=1)$, on the assumption that lines closer to the core are less affected by the non-Gaussian wings.

No lines coming from levels $v''=2, J''=3$ or $J''=4$ are detected: pumping lines for these levels are not present in the $H_{Ly\alpha}$ profile. As Figure 8 makes evident, no lines originating from the far blue side of the $H_{Ly\alpha}$ line are observed either. We have searched for strong

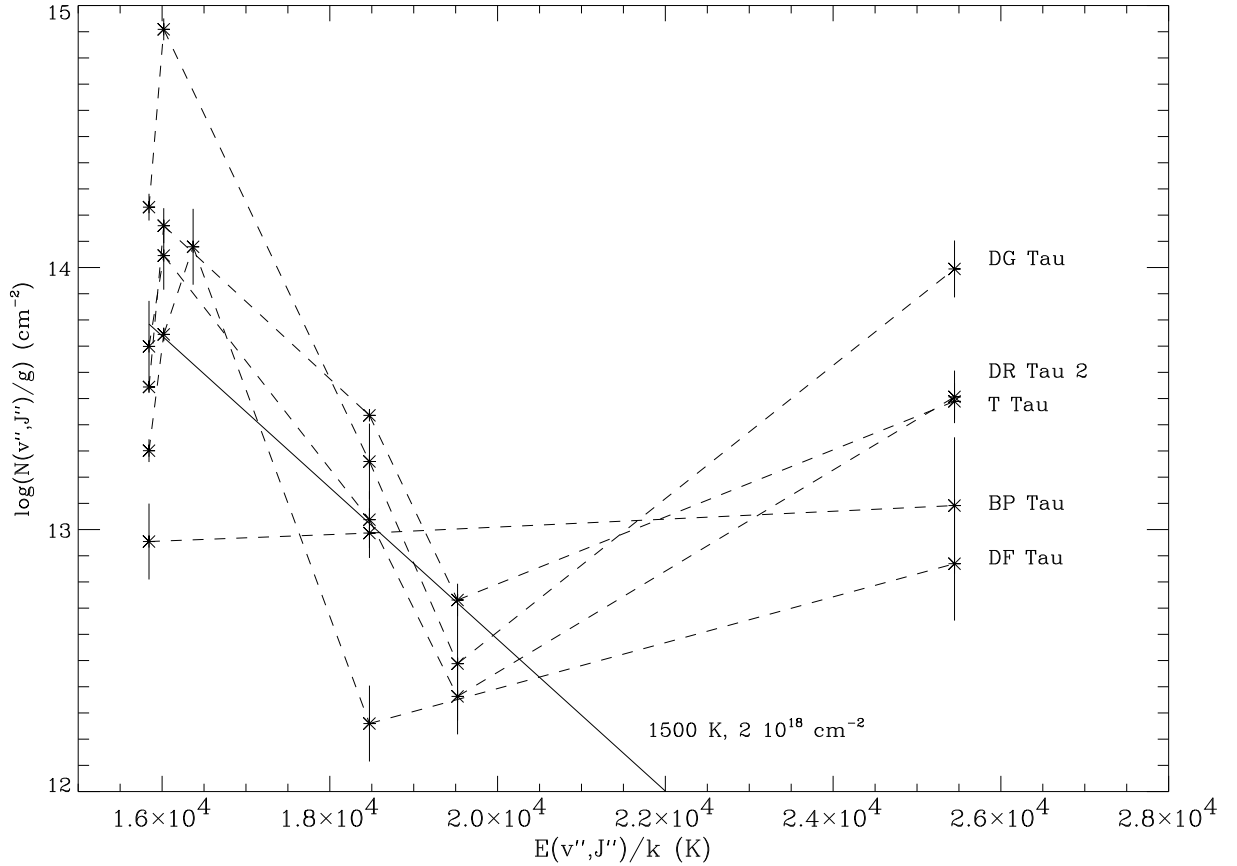


Fig. 9.— Distribution of level populations for some of the stars in our sample (dashed lines). The ordinate is the logarithm of the column density of H_2 molecules (in a given v'', J'' level), divided by the g'' of the level (where we assume an ortho/para ratio of 3). The abscissa is the energy of the level in degrees Kevin. The solid line indicate the expected locus from a thermal distribution at 1500 K and total H_2 column density of $2 \times 10^{18} \text{ cm}^{-2}$.

lines with exciting transitions to the blue of $H_{Ly\alpha}$, originating from low molecular levels, that should be observable in our spectra. We find three candidates: $(v'', J'')=1, 15$ ($R(15)3-1$ at -300 km s^{-1}), $(1, 11)$ ($P(11)1-1$ at -800 km s^{-1}), and $(1, 12)$ ($R(12)1-1$ at -780 km s^{-1}). There are other possible lines which would produce H_2 emission in our spectral ranges, but they originate in states with higher excitation energies. The line closest to the center, if we assume a population similar to that of $v''=1, J''=13$ should produce fluoresced lines stronger than those produced from $P(13)2-1$, as its A -value is $1 \times 10^8 \text{ sec}^{-1}$. The fact that we do not see such lines may be an indication that excitation of H_2 by $H_{Ly\alpha}$ occurs far enough from the star such that the blue wing of $H_{Ly\alpha}$ has already been absorbed by the wind. This picture can be tested with data having better signal-to-noise and wider spectral range, which will allow to decide whether or not lines coming from the blue side of $H_{Ly\alpha}$ are excited by an absorbed profile. At this point, we can say that the asymmetry in the excitation routes is tantalizing but needs more study.

As argued above, the result that the populations of H_2 are not in thermal equilibrium does not depend strongly on the exact shape of $H_{Ly\alpha}$, as long as the flux decreases to the red, from the rest wavelength (this is implicit in the assumption that $H_{Ly\alpha}$ is a Gaussian at 1215.67 \AA). From the Blondel et al. (1993) observations, it is not clear that this is so. The observed $H_{Ly\alpha}$ line in the very noisy, underexposed IUE spectra is to the red of the rest wavelength. If the $H_{Ly\alpha}$ profile absorbed by H_2 were redshifted (either because its blue wing is absorbed by a wind, or it is emitted in a moving region), the conclusion that the populations are not in thermal equilibrium would need to be revised, as exciting lines close to the nominal line center would see less $H_{Ly\alpha}$ flux, which would translate in larger measured populations. This will tend to erase the minima observed Figure 9, which are due to levels very close to the nominal center of $H_{Ly\alpha}$. On the other hand, it seems difficult to alter the very flat appearance of the trace of BP Tau in Figure 9 by changing the shape of $H_{Ly\alpha}$.

What can these observations tell us about the excitation mechanism and the origin of the H_2 emission? Two kinds of heating mechanisms are generally proposed: heating by absorption of part of the stellar and accretion luminosity (including X-rays see Weintraub, Kastner, & Bary 2000), and heating by dynamical processes, including shocks, and turbulent decay. Very little has been published about the expected populations of H_2 in CTTS. A preliminary model by Black & van Dishoeck (1987) shows that highly excited states of H_2 can be produced (by UV radiation) assuming that the populations in $v'' \leq 2$ are in thermal equilibrium at 2000 K. ISO observations of IR lines in T Tau by van den Ancker et al. (1999) are consistent with a C-shock that rises the gas temperature to 1500 K. The same ISO observations indicate the presence of a 440 K H_2 gas and conclude that yet another very low temperature component must be present to explain the total gas mass derived from CO observations. Figure 9 shows that, while a temperature in the range of 1000 to 2000 K may

be appropriate, the assumption of LTE is not true.

The fact that the average velocities of the measured H₂ lines are all blueshifted suggests that the emission comes from an outflow, as opposed to the disk surface layers or its inner edge. This conclusion is reinforced by the fact that the detected profiles are single peaked. Given the instrumental resolution, we should detect double peaked profiles if the emission comes from material within $\sim 10(M/0.5M_{\odot}) \sin^2 i$ AU, where M is the mass of the central star and i is the inclination angle. We do not see such profiles, which implies that if the emission comes from the disk, is either originating beyond this limit or comes from a wide range of disk radii. In spite of the model uncertainties, it is clear that a large temperature, of the order of 1000 K, is necessary to produce the observed excited states from which H₂ will be pumped. At these distances in the disk, the temperature due to reprocessed stellar radiation should be much less.

Analysis of forbidden(HEG95) wind diagnostics in CTTS indicate that wind temperatures are ~ 8000 K and densities are $\sim 10^5$ cm⁻³. These values suggest that if the H₂ emission comes from this same flow, it should be originated in the outer, cooler and less dense parts of it (assuming a length scale of the order of one stellar radius). Therefore, the wind origin of the emission is plausible, but more observations (for example, long-slit spectroscopy) are needed before we can really understand its distribution.

4.2. Blending of Si IV and C IV with H₂

As mentioned in the introduction, the C IV and Si IV doublets are affected by overlying lines of H₂. Such lines will affect any low-resolution measurement of the doublets. In this section we will separate the emission due to H₂ from that due to C IV and Si IV. Some of the results from section 4.1 are based on these extractions.

Figures 10 and 11 show the Si IV and C IV doublets. Notice that the separation between the two members of the C IV doublet is ~ 500 km s⁻¹, and so in the red side of the thick trace (or the blue side of the thin trace) one sees the beginning of the other member. Figures 13 and 14 show the same doublets after subtracting the H₂ emission.

The blue member of the Si IV doublet is affected by R(0)0-5 (at 1393.719 Å) and R(1)0-5 (at 1393.961 Å). The red member is affected by P(3)0-5 (at 1401.648 Å). These H₂ lines are responsible for the redshifted peak of the blue line and the blueshifted peak of the red line. The red member of the C IV line is affected by R(3)1-8, which can be seen most clearly in the blue shoulder of the blue line of C IV in BP Tau. We have searched the Abgrall et al. (1993) database for other lines affecting the doublets and we conclude that in our spectra

these are the most important lines. Using the fact that these H_2 lines are optically thin, we can use other lines from the same upper level to obtain estimates of their fluxes. We start with an analysis of the Si IV doublet, followed by the C IV doublet.

R(0)0-5 and P(2)0-5 come from the same upper level and the flux from P(2)0-5 is expected to be twice as large as that from R(0)0-5. We can measure P(2)0-5 with confidence given that it is isolated between the two members of the Si IV doublet. Given the size of the P(2)0-5, contribution of R(0)0-5 to the blue member of the Si IV profile is negligible in most cases. R(1)0-5 and P(3)0-5 belong to the same fluorescent route, and the later is expected to be 1.4 times more intense than the former. For T Tau, DF Tau and DR Tau, we have additional spectral ranges that allow us to determine the contribution of H_2 to the doublet from other H_2 lines present in the spectra from the same fluorescent route. In Figure 12 we indicate how is the decomposition performed. For BP Tau, RW Aur, RY Tau, RU Lup, and DG Tau, these are the only strong lines from this fluorescent route present in the spectra. Therefore, to obtain estimates of their influence in the Si IV profiles, we need to resort to indirect methods. As we argue below, we make positive detections of Si IV only on BP Tau, RU Lup, RW Aur, and T Tau. In the case of HBC 388 there is no indication that the Si IV lines are affected by H_2 emission. Such emission, if present, is buried under the noise for all H_2 lines identified reliably in other stars. We now indicate how to carry out the deblending procedure for some individual stars.

For those stars without additional members from the same route as R(1)0-5 and P(3)0-5 we estimate their intensities by the following reasoning. In STIS spectrum of TW Hya (Herczeg et al. 2001), the ratio between the peak values of P(2)0-5 and R(1)0-5 is ~ 0.7 . If one assumes this ratio is the same for all CTTS, from the measured flux of P(2)0-5 we obtain R(0)0-5 and R(1)0-5, and then P(3)0-5. The comparison with TW Hya is useful because, if H_2 is due to $H_{Ly\alpha}$ fluorescence, both P(2)0-5 and R(1)0-5 are excited from $v'' = 2$ and their excitation wavelengths are $\sim 100 \text{ km s}^{-1}$ apart, so the H_2 populations feels a similar $H_{Ly\alpha}$. If the FWHM of the $H_{Ly\alpha}$ emission for a star in our sample is larger than that of TW Hya, the ratio of the two lines would be closer to 1. This is the case for DG Tau, for example. We have ignored this complication and assume the same ratio always. Alternatively, we could use the populations derived in section 4.1 to obtain estimates of the line ratios for the two different routes. Such procedure produces similar results (within the errors) as the one outlined here.

For BP Tau, the contamination of Si IV by H_2 is not very important. Given the strength of P(2)0-5, R(0)0-5 should be within the noise level. Using TW Hya we conclude that R(1)0-5 and P(3)0-5 are at noise level. For BP Tau star, the values of Si IV in Table 3 are obtained without any correction for H_2 . In the case of RY Tau, a similar argument implies that

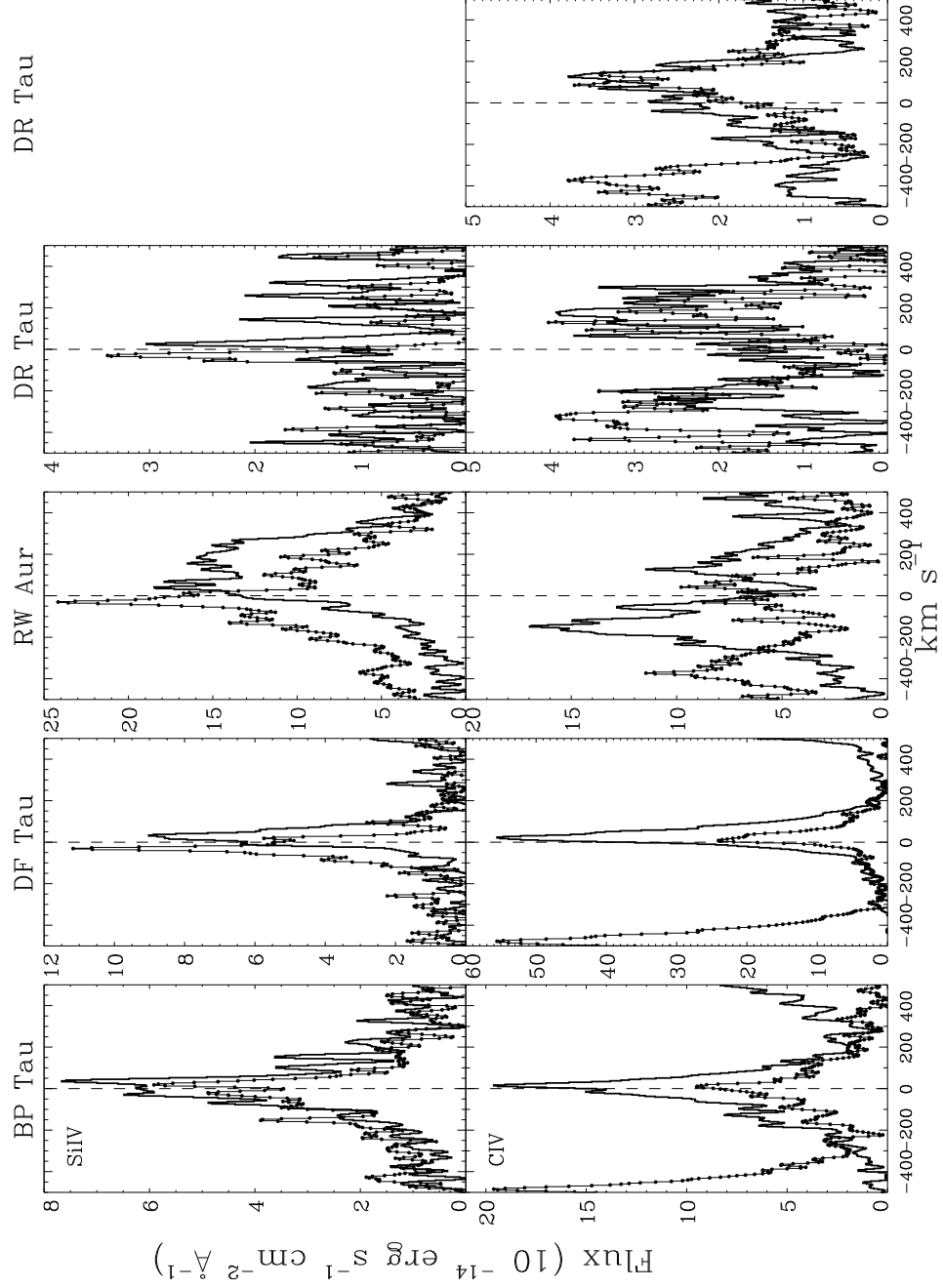


Fig. 10.— Doublet plots (Si IV and C IV). All the spectra have been smoothed. The thick (thin dotted) line indicates the optically thicker (thinner) member of the doublet. For these doublets, the optically thicker line is always the blue one. Zero velocity is indicated with a dashed line for all lines.

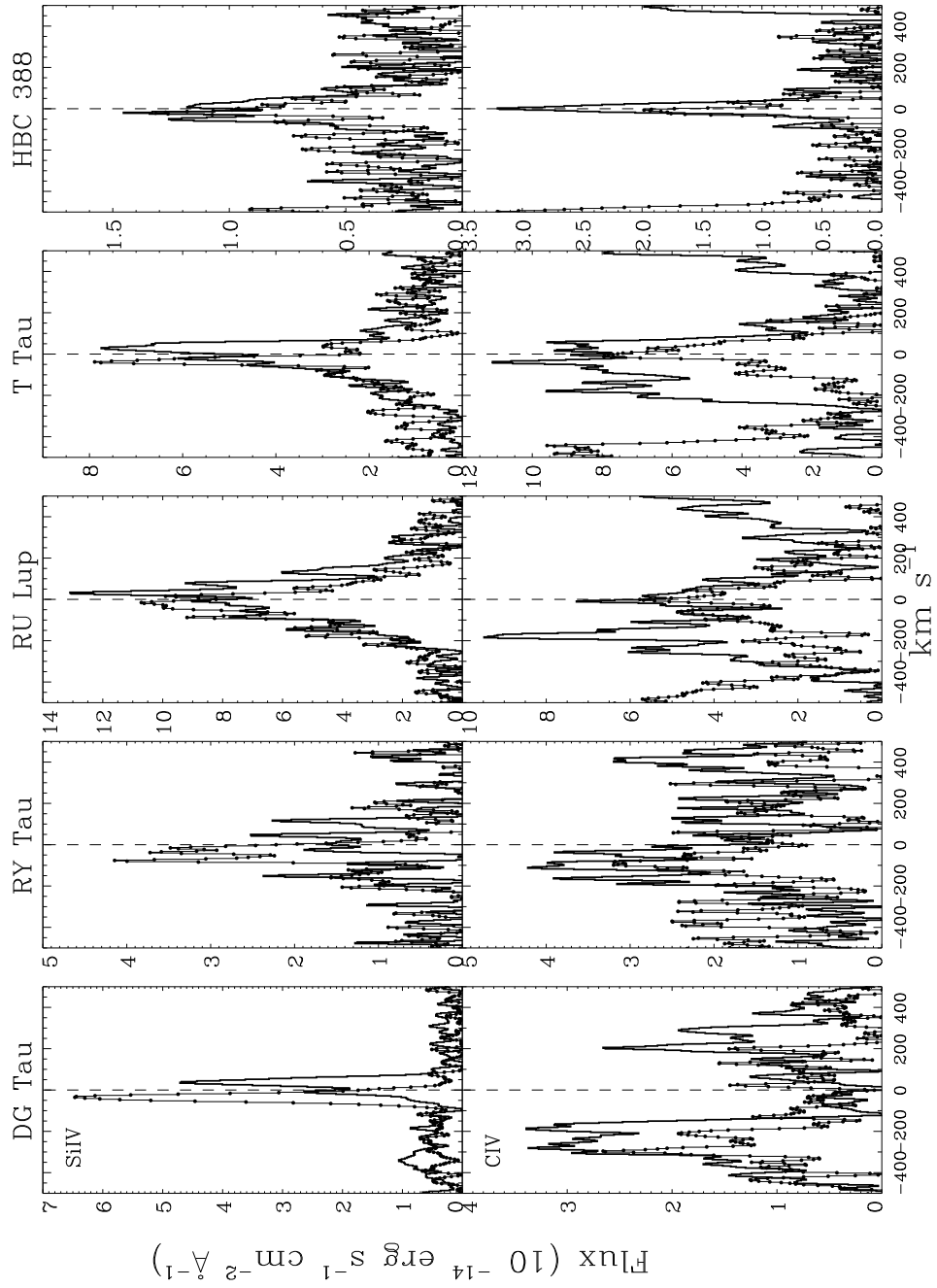


Fig. 11.— Doublet plots (Si IV and C IV), cont.

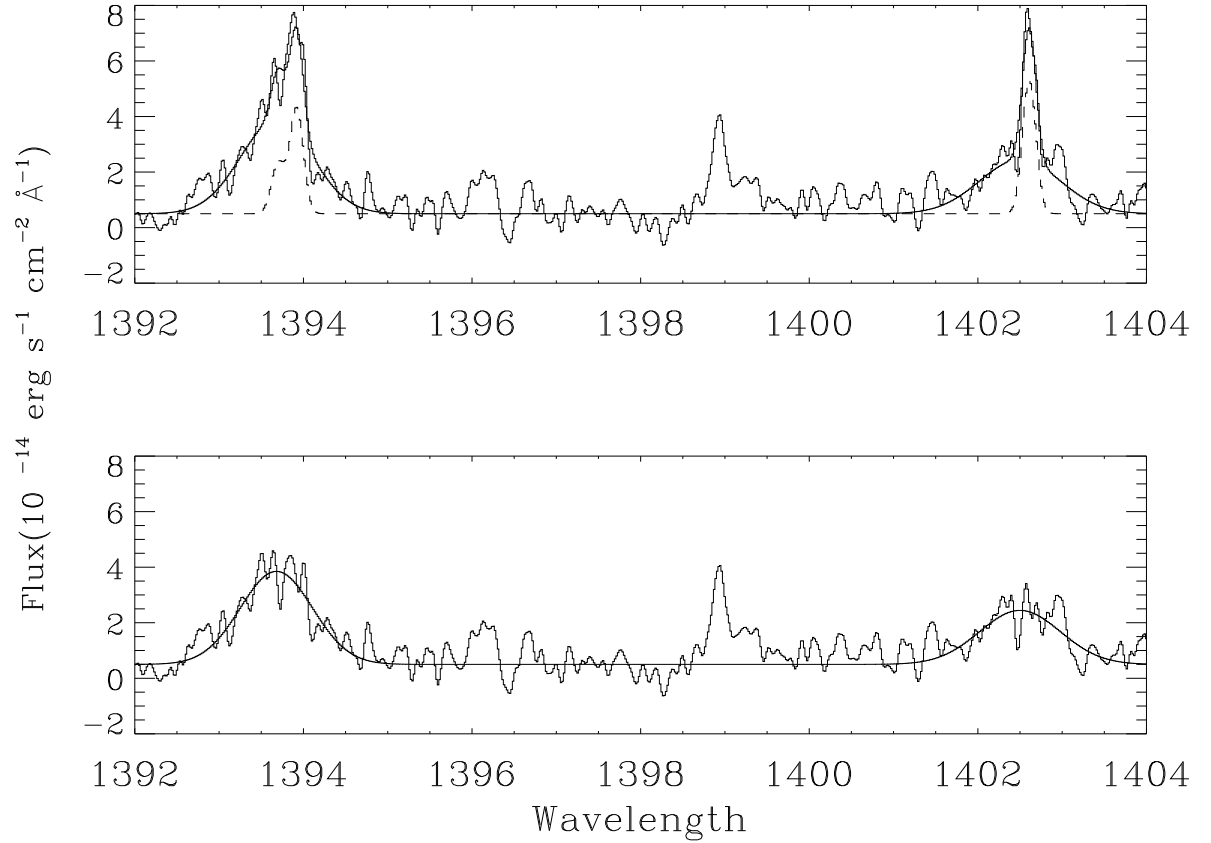


Fig. 12.— Example of deblending procedure for T Tau. The Figure shows the wavelength range that contains Si IV. The data are the jagged lines. In the top plot is the observed spectrum. The dashed line is the contribution from H₂ (Lines R(0)0-5, R(1)0-5, and P(3)0-5). We have obtained the strength of these lines and widths for these lines from other lines in the same fluorescent route (see Table 4), assuming that all are optically thin. The centroids are obtained by averaging the centroids of other lines in the same route. The bottom plot shows the data after subtracting the H₂ contribution. In both plots, the smooth solid line is the fit to the spectra, before (top) and after (bottom) subtraction.

whatever we see in the neighborhood of the Si IV doublet is due to H₂. For RU Lup, the fact that the blue line is stronger than the red one (unlike what is observed in pure H₂ emission) implies that some Si IV must be present, which we indicate in Table 3. In the case of RW Aur, the red H₂ emission is clearly visible, superimposed to the broad Si IV emission. We use the measured parameters to obtain the blue H₂ line.

For DG Tau, sharp emission peaks are present at the position of the Si IV doublet. Their positions coincide with those of R(0)0-5, R(1)0-5 and P(3)0-5. Their width is similar to other H₂ lines in the spectrum, like P(5)1-8. The ratio of the peak emission in the red Si IV line to the peak emission in the blue Si IV is ~ 1.5 as expected if they are optically thin H₂ lines. The same is true for P(2)0-5 and the blue peak of the blue Si IV line. Note that the P(2)0-5 and R(1)0-5 lines have approximately the same flux, which implies the H_{Lya} emission is wider for this star than for TW Hya. We conclude that the emission in the Si IV wavelengths is due to H₂.

DF Tau presents a difficult case. As mentioned in section 4.1 if one identifies the lines near Si IV wavelengths as being just R(0)0-5 and P(3)0-5 (i.e., assuming no Si IV), the resulting lines are very wide and do not have the expected intensity of optically thin lines. On the other hand, using the two other available lines in the same fluorescent route to predict their intensity, absorbs most of the lines in the 1400 Å region. This indicates that Si IV emission is present, but at the noise level. The upper-limits for Si IV quoted in Table 3 will contain all the flux.

The C IV doublet is contaminated mainly by R(3)1-8, which should have similar strength to P(5)1-8, assuming both are optically thin. No other H₂ lines are strong enough to affect the C IV doublet. Furthermore, the effect of other atomic lines in the C IV doublet members is negligible. Errico et al. (2000) have argued that the shapes of the profiles in RW Aur are due to absorption by Fe II in the wind (see next section). If this is true for other stars, we should detect a similar pattern of absorptions, and we do not. Furthermore, Sandlin et al. (1986) show that in the Sun one observes strong Si I lines in this region. As the signal-to-noise in this region of our spectra is not very high, it is possible that some Si I lines are present. We searched for these lines and obtained estimates of their strengths, using other lines of the same multiplets present in the spectra. We conclude that the contribution of Si I to the C IV profiles is negligible. We detect C IV in all the stars.

The spectra from DG Tau show strong blueshifted features in both lines. The subtraction of R(3)1-8 does not alter the appearance of the doublet very much. The signal-to-noise of the features to the red of the red member (Figure 11) is close to 1, so they are not significant. The fact that both members show emission at similar velocities lead us to conclude that the emission is indeed due to C IV. The signal-to-noise in the region is close to two, so

the double peaked structure is not significant.

4.3. The Si IV and C IV Profiles with no H₂

4.3.1. Morphology

In this section, we study the profiles resulting from subtracting the H₂ contribution (Figures 13 and 14). In particular we are interested in the process responsible for the shape (width and components) and the origin of the transition region lines. The C IV line profiles show a wide array of shapes, from the centrally peaked emissions of DF Tau to the very asymmetric ones of DG Tau and DR Tau.

DR Tau shows a remarkable variation in C IV from the first to the second epoch of observations. The first epoch shows a blueshifted emission at ~ -250 km s⁻¹ separated from the main blue peak (Figure 15). Furthermore, for the first epoch, the blue peak shows a red excess when compared to the red peak. Such excess is absent from the second epoch, as is the blueshifted emission at ~ -250 km s⁻¹. We interpret this morphology as a transient event in the first epoch. This event produced C IV emission 250 km s⁻¹ to the blue of both C IV lines. The apparent excess to the red of the blue line actually belongs to this event in the red line. Without this extra emission the red and blue lines in both epochs look remarkably similar. In Table 3 we have decomposed the C IV lines from the first epoch in a blue and a redshifted component (see section 4.3.3).

Table 6 summarizes the results of our measurements and compares them with those obtained by Valenti et al. (2000), who use average low resolution IUE data. IUE data can barely resolve the two members of the Si IV doublet, but not the C IV doublet. Also, it cannot be used to subtract the contribution of H₂ to these lines. As Table 3 shows, this correction is small, $\sim 10\%$ or less in all cases. A similar estimate was obtained by Johns-Krull et al. (2000), using the much larger IUE aperture.

In the Table we quote upper limits for the Si IV that we cannot measure. These upper limits are twice the value obtained by integrating a smoothed noise vector over the same width as the C IV line. As such, they are the flux of a line with this FWHM and correspond to a 2- σ detection. From Table 6 it is clear that the intrinsic variability of TTS dominates over any H₂ correction. For example, the C IV flux in DF Tau increases by a factor of 2, while the flux in RU Lup decreases by a factor of 5, with respect to the measurements of Valenti et al. (2000).

For stars in which we have both C IV and Si IV profiles, we observe two different

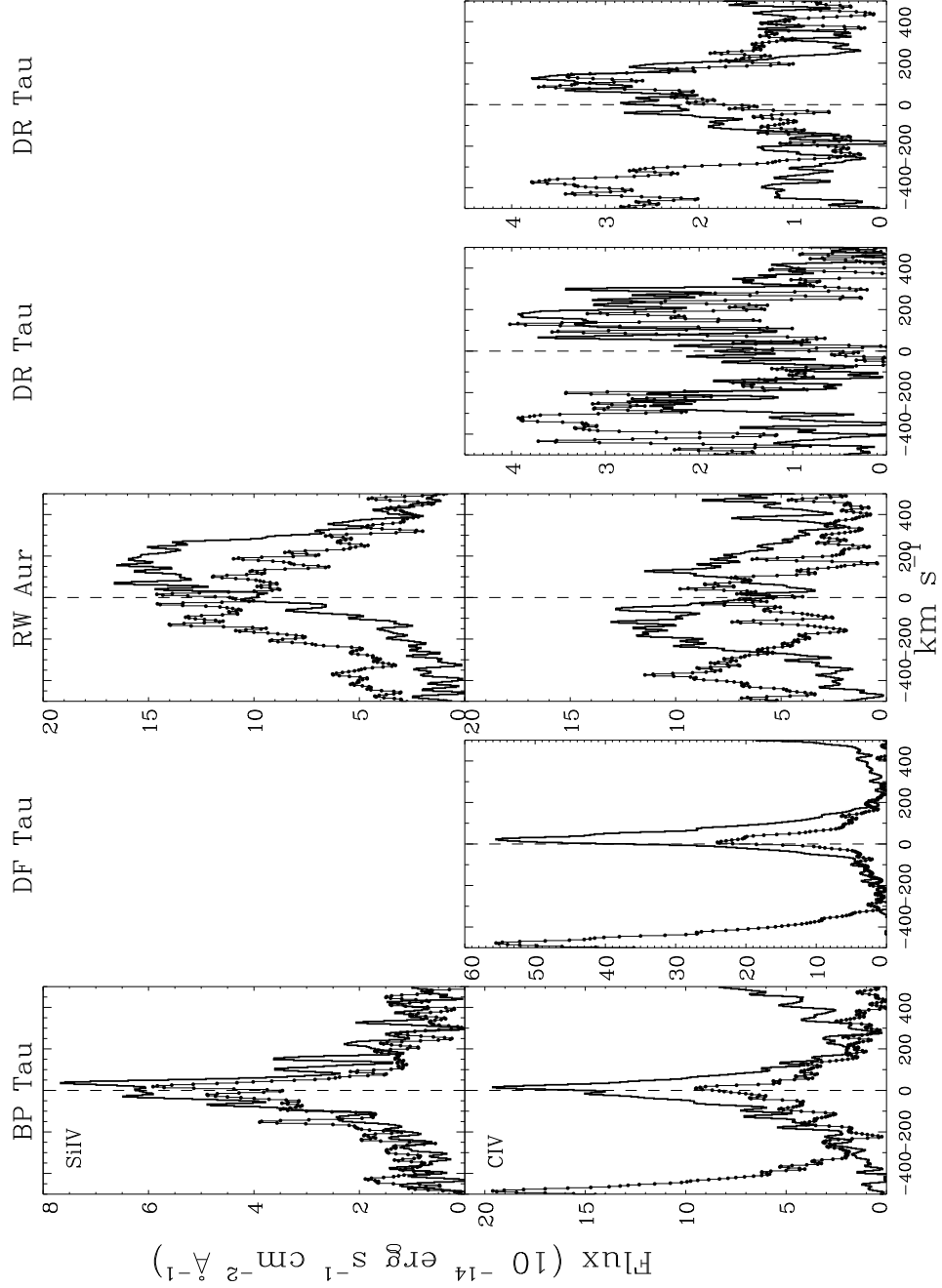


Fig. 13.— Doublet plots (Si IV and C IV), with H_2 subtracted. The conventions are the same as in figures 10. Note that the vertical scale has changed. Blank spaces indicate stars for which the subtraction of the H_2 lines produces profiles consistent with noise (i.e., profiles in which no Si IV is detected).

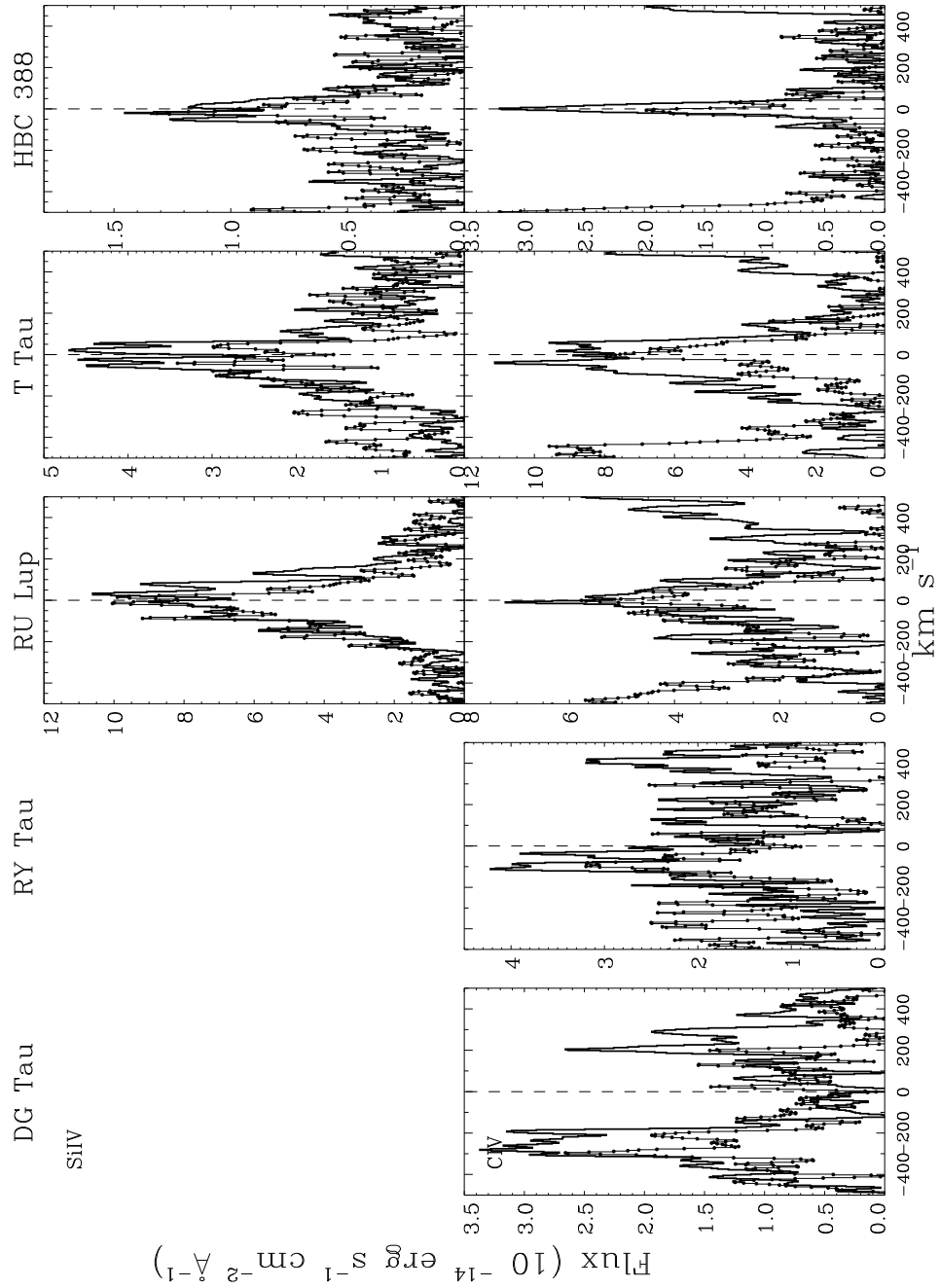


Fig. 14.— Doublet plots (Si IV and C IV) without H₂, cont.

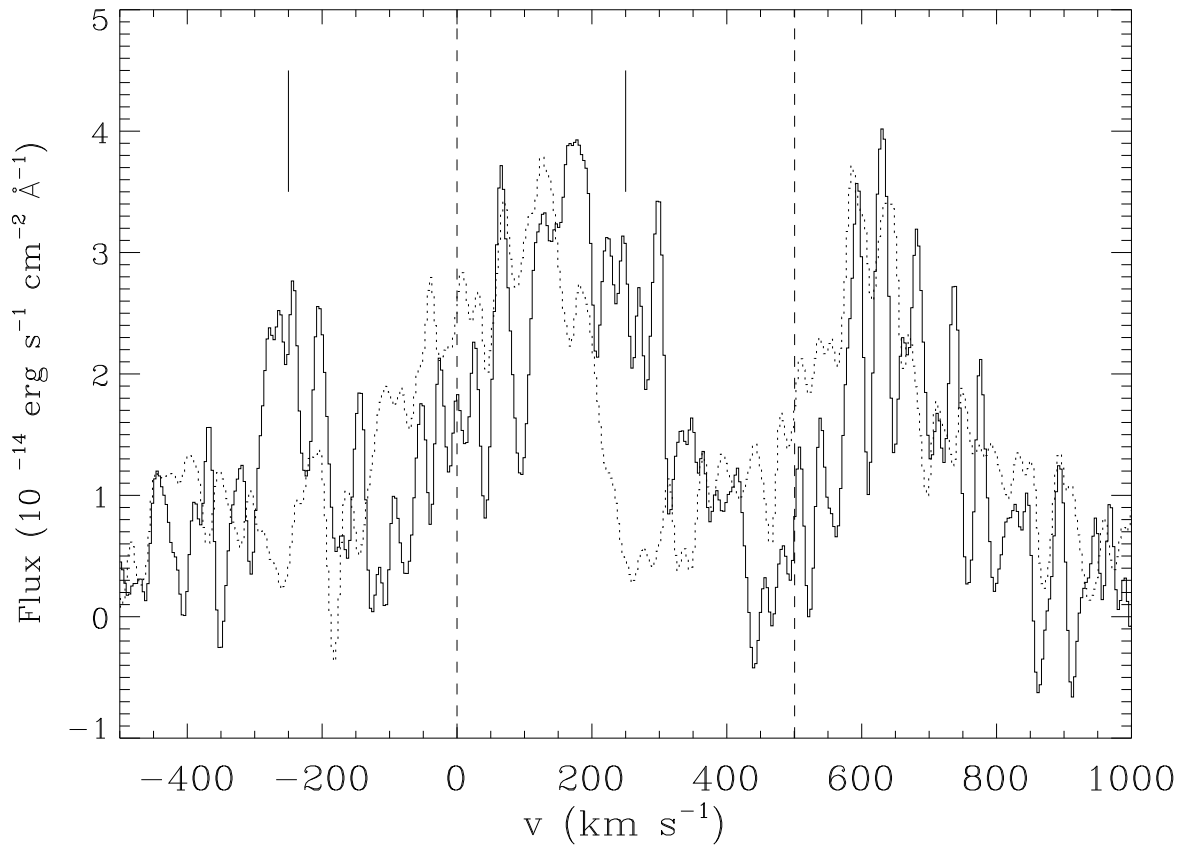


Fig. 15.— C IV profiles for DR Tau. We have subtracted the contribution from R(3)1-8. The solid (dotted) lines is the first (second) epoch of observations. The velocity scale is centered on the blue member of the doublet. The vertical dashed lines indicate the position of the doublet members. The vertical solid lines indicate the positions of the transient emissions in the first epoch profile.

Table 6. Fluxes of Transition Region Lines

Name	This Work		Valenti et al. 2000	
	Si IV	C IV	Si IV	C IV
BP Tau	6 ± 1, 4 ± 1	24.0 ± 0.8	4.9 ± 0.2, 3.9 ± 0.3	25.2 ± 0.4
T Tau	3.6 ± .4, 2.2 ± 0.4	17 ± 1	7.3 ± 0.6, 5.9 ± 0.6	44.5 ± 0.9
DF Tau	< 4, < 4	45.7 ± 3	4.4 ± 0.1, 3.3 ± .1	25.2 ± 0.4
RW Aur	19 ± 2, 25 ± 2	23 ± 6	12.9 ± 0.5, 10.7 ± 0.5	21 ± 1
DG Tau	< 1.3, < 1.3	4.3 ± 0.4	1.4 ± .2, 1.1 ± .2	5.0 ± 0.6
DR Tau	< 1.5, < 1.5	6 ± 1, 5.6 ± 0.4	2.5 ± .1, 2.7 ± 0.1	17.3 ± 0.6
RY Tau	< 2, < 2	4.2 ± 0.5	1.64 ± 0.07, 2.90 ± 0.07	8.7 ± 0.3
RU Lup	10.8 ± 0.7, 8.5 ± 0.6	14 ± 1	27.2 ± 0.7, 19.8 ± 0.7	76 ± 1
HBC 388	0.7 ± 0.1, 0.4 ± 0.1	1.4 ± 0.2

Note. — All the fluxes are in units of 10^{-14} ergs sec $^{-1}$ cm $^{-2}$. The fluxes are not corrected for reddening. In the Si IV columns, both members are quoted separately. In the C IV columns relating to this work, the fluxes in each member of the doublet have been added. We have two different epochs for DR Tau C IV

behaviors in the ratio of their fluxes. For BP Tau, T Tau and HBC 388, the C IV blue line is stronger than the Si IV blue line. For RW Aur and RU Lup, the situation is reversed. As comparison with the SUMER Atlas of Solar-Disk features shows³, the flux ratio of C IV to Si IV can change from ~ 0.7 to ~ 4 as one goes from the network to the quiet Sun (Curdt et al. 2000). In our target stars the ratio from C IV to Si IV varies between 0.4 (RW Aur) to more than 5 (DF Tau). The number of stars for which we actually measure both lines is small (only four CTTS, for which we get that the average ratio of C IV to Si IV fluxes is 1.3), and so it is difficult to explain the cause of these differences. The relationship between the C IV and Si IV emission is clarified by Figure 16, which shows an almost linear correlation between the two. Therefore the flux in C IV predicts the flux in Si IV. C IV and Si IV fluxes are also correlated in stellar chromospheres (e.g. Ayres, Marstad, & Linsky 1981).

Figure 17 compares the Si IV and C IV red members for those stars for which we have both, not including RW Aur (we discuss the RW Aur case below). The Si IV and C IV profiles look very similar to each other in all stars, which indicates that they are formed in the same region. For HBC 388, the Si IV line is broader than the C IV line. This is unlike SUMER observations of the Sun, for which both lines are very similar. The Si IV and C IV observations are not simultaneous, so it is not impossible that a flare event is affecting the Si IV observations of HBC 388.

The Gaussian fits to the Si IV and C IV profiles, indicated in Table 3, show that the widths vary from ~ 200 to ~ 300 km s $^{-1}$. For BP Tau and DF Tau the signal to noise is high enough to perform a decomposition in multiple Gaussian elements. In the case of BP Tau we perform a two element Gaussian decomposition to each line, which results in a NC and a BC. For DF Tau, we perform a 3 element Gaussian decomposition of the C IV profile. In general, we find a BC of width ~ 300 km s $^{-1}$ and a NC of width ~ 100 km s $^{-1}$. For DF Tau we also find a narrower component with width ~ 50 km s $^{-1}$. Multiple components may indicate that the emission comes from more than one region: for example, the NC may come from the post-shock while the BC comes from the pre-shock. On the other hand, the shape of the line may be the result of the area of the accretion ring oriented towards the observer (Section 4.3.3) and so a Gaussian decomposition is not really valid.

In these analyses RW Aur stands in a class by itself. Not only are the C IV and Si IV lines very different to each other, but the individual members of each doublet are very different among themselves. Errico et al. (2000) have analyzed the C IV doublet for RW Aur and they conclude that its appearance can be explained by Fe II absorption from a 10000K stellar wind. For this explanation they invoke FeII] absorption, together with permitted FeII lines.

³http://www.uio.no/~paalb/sumer_atlas.html.

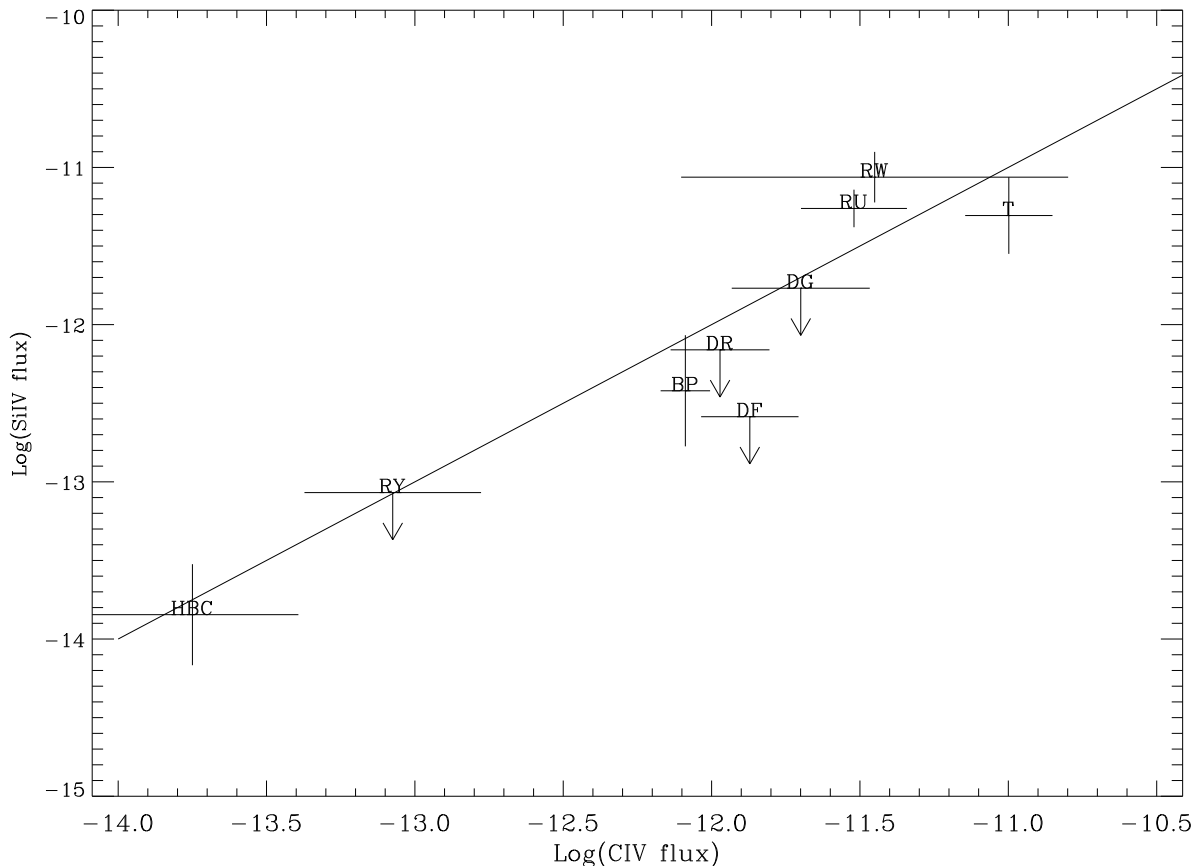


Fig. 16.— Si IV vs. C IV. The bars indicate errors. Upper limits are indicated by arrows. The solid line is the identity relationship.

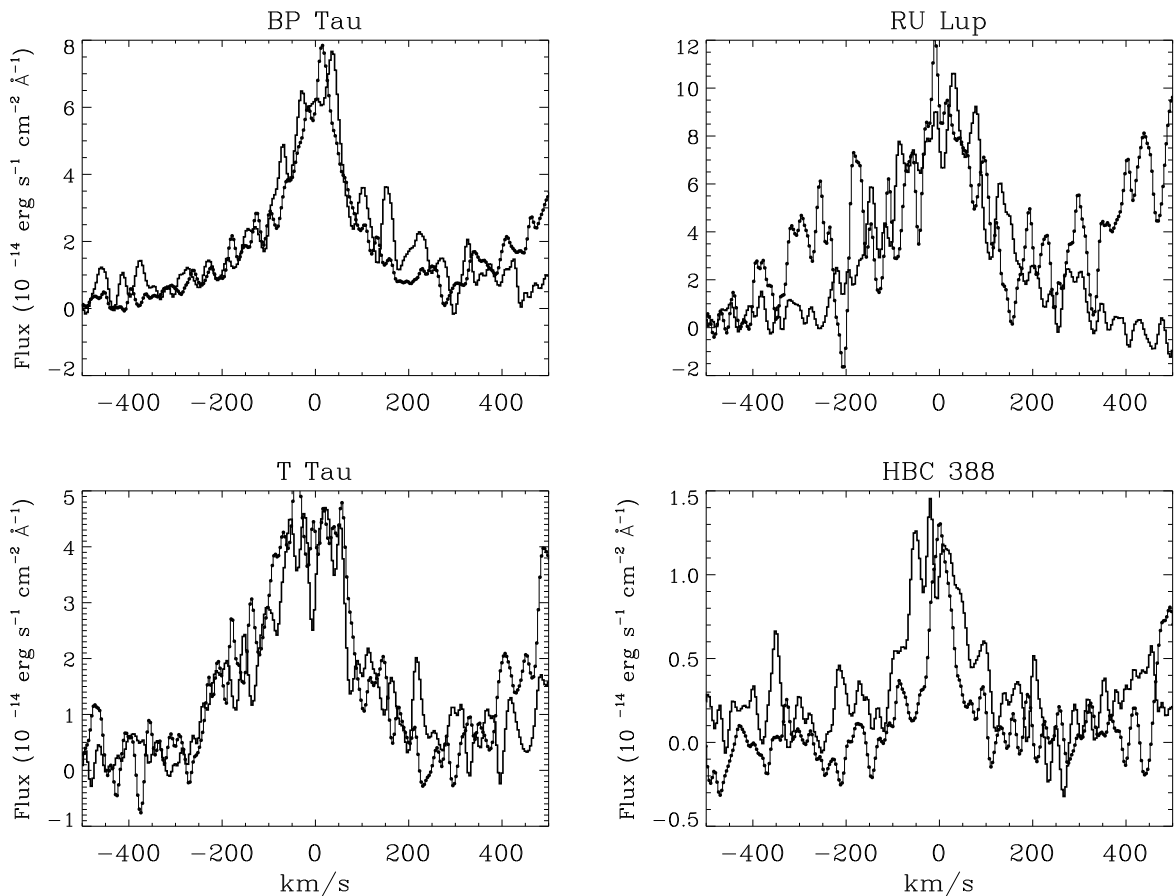


Fig. 17.— Comparison between the red members of Si IV (thick) and C IV (thin dotted). The C IV lines have been scaled to match the peak of the Si IV in each star.

Without more careful modeling of the wind environment of RW Aur is not clear if this is the correct explanation, especially since nearby FeII] lines are absent. The red Si IV line may be affected by O IV], and both members are affected by Fe II. We do not observe any other example of these Fe II absorptions (or emissions) in the other stars in our sample (although Lamzin 2000a reports strong Fe II features in RU Lup, in the 2325 Å range), which may indicate that RW Aur has the coolest and/or densest wind of all our stars. Without higher resolution and higher signal-to-noise spectra to disentangle the contribution of Fe II lines to the RW Aur spectrum, it is premature to advance any definite conclusion.

4.3.2. *Relationship to Accretion*

We have seen that the Si IV flux is correlated with the C IV line flux. We know show that the C IV line flux is also correlated with the intensity of H₂ and therefore can be used to predict the overall appearance of the spectra.

We observe a correlation between C IV and H₂ (Figure 18, top plot). In the Figure we use the H₂ line P(5)1-8 at 1562.39 Å. While this line is weak in most of our spectra, it is present in all of them. For C IV we sum the flux in both elements of the doublet (once they have been corrected for H₂ emission). For an individual star, a correlation between multiple observations of C IV and P(5)1-8 is expected, because even with no accretion H_{Lyα} and C IV are both indicators of accretion activity. It is surprising, however that we observe the correlation for multiple stars. This indicates that what limits the emission is pump photons, not the state of H₂ or the stellar inclination.

In the CTTSs, the fluxes from Si IV, C IV, and H₂ are most likely driven by the accretion rate. To understand what fraction of emission in the transition lines of CTTS is due to accretion processes we can look at HBC 388. This is a WTTS and so the emission in C IV and Si IV is not related to accretion processes. It is a fairly massive TTS, with one of the smallest radii in our sample. The emission is very weak. If all the stars shared the same intrinsic line surface flux, the observed unreddened fluxes would scale with their respective surface areas. In Figure 18 (middle) we show the ratio between the observed C IV flux and the predicted one, assuming that all the stars have the C IV surface flux of HBC 388. For RY Tau and T Tau, which are stars of similar spectral type as HBC 388, this assumption underpredicts the observed C IV flux by a factor of 2 and a hundred, respectively. On the basis of the Figure we conclude that the C IV flux is dominated by accretion-driven emission processes, as opposed to solar-like stellar chromospheric activity, even though at low accretion rates the chromospheric contribution becomes important. The accretion process has enough energy to drive the emission, as the luminosity in C IV is only a small fraction (<0.1%) of

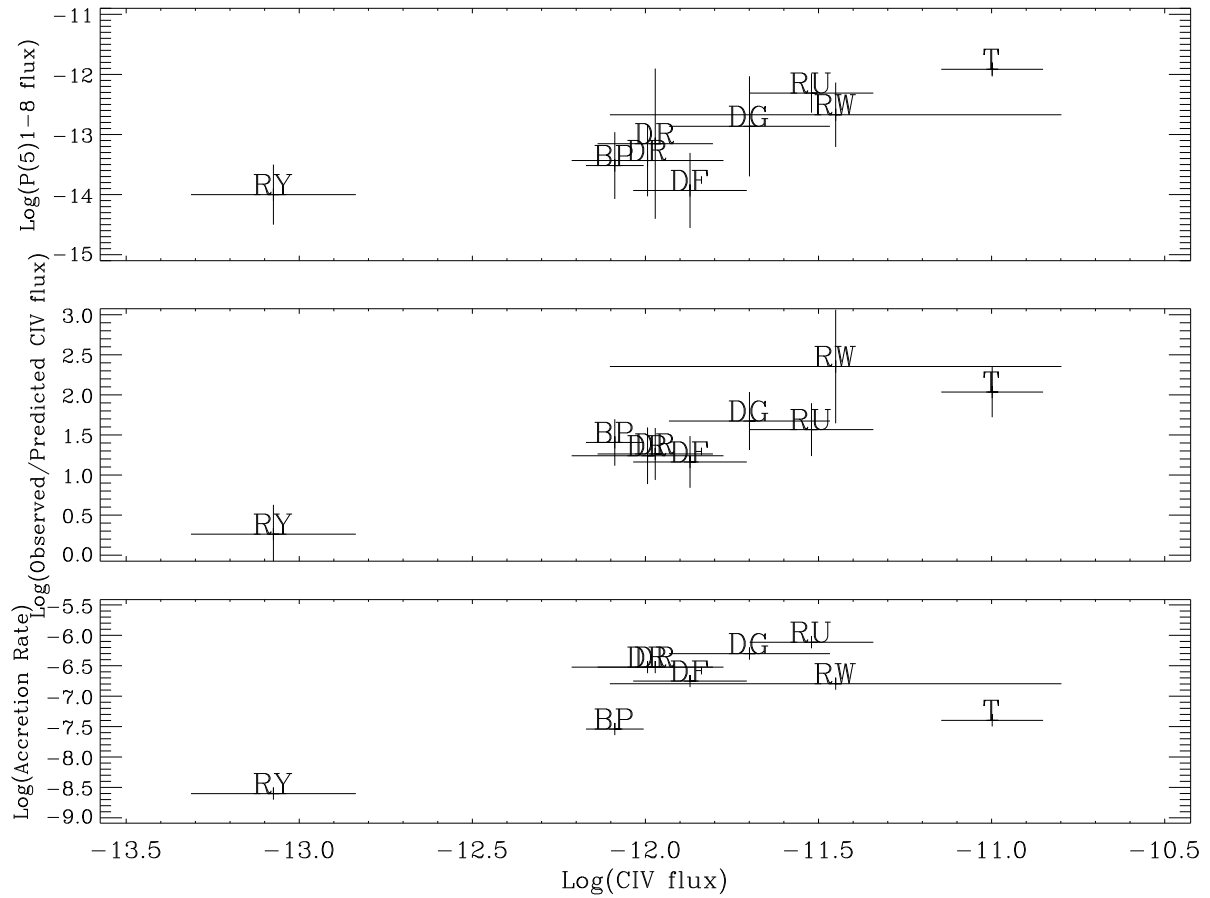


Fig. 18.— Relationship between C IV doublet flux (corrected for H₂ and extinction) and the flux of the H₂ line P(5)1-8 (top), the ratio of observed to predicted C IV fluxes (middle), and the accretion rate (bottom).

the accretion luminosity (Calvet et al. 1996). It should be kept in mind that the internal structure of HBC 388 (a K1 star) may be different from that of lower mass stars in our sample (which are K7 or later), and so it is not clear how representative the chromospheric emission of this WTTS is.

Figure 18 shows the relationship between C IV and accretion rate. It should be noted that a relationship similar to this one is obtained by Johns-Krull et al. (2000). On the basis of such relationship, they conclude that the accretion rate for T Tau is $30 10^{-8} M_{\odot}/\text{yr}$. Using this accretion rate the point for T Tau in Figure 18 moves upward to the position of RW Aur. This Figure certainly suggests that accretion is the single engine behind the strong hot lines.

4.3.3. *The origin of the hot line emission*

In this section we study what the line shapes can tell us about the emission line region.

As Muzerolle, Hartmann, & Calvet (1998) argue on the basis of the appearance of the NaD and Balmer lines, the temperature in the funnel flow is around 10000 K. Therefore, the C IV and Si IV lines cannot originate in the funnel. The shock region itself and the stellar atmosphere are prime candidates for being the source of the emission. In the shock at the end of the accretion funnel there are two different regions that may contribute to the emission: the pre-shock or radiative precursor, and the post-shock. The former has velocities of $\sim 300 \text{ km s}^{-1}$ and temperatures $\sim 10^4 \text{ K}$, while immediately after the shock the velocities are $\sim 70 \text{ km s}^{-1}$ and the temperatures are 10^5 K (Calvet & Gullbring 1998). Both regions may emit hot transition region lines. The shape of this shock on the surface of the star is unknown: assuming a dipolar magnetic field produces a ring on the stellar surface.

The ratio between the emission from the radiative precursor and that from the post-shock depends on the velocity, according to Lamzin (1998), in such a way that the post-shock dominates for infalling velocities larger than 300 km s^{-1} (at infalling densities of 10^{12} cm^{-3}). The post-shock emission is produced at very low velocities. In general, one should therefore observe a broad redshifted component (the pre-shock emission) and a narrow centered component. For DF Tau and BP Tau, the only stars for which a decomposition in multiple components is possible this is not observed. More generally, as infalling velocities are almost certainly less than 300 km s^{-1} , pre-shock emission which preferentially produces redshifted profiles, should dominate. This is an attractive possibility because the emission should be broad. However, from Figures 13 and 14, four stars in our sample have centered profiles, which suggests that a different region is responsible for the emission.

Lamzin (2000c) modeled the effect of the ring geometry in the Si III] line (1892 Å. When collisionally excited in a low density medium, the ion is formed at 30000 K, see Arnaud & Raymond 1992) for RY Tau and RU Lup, using the spectra shown in Figure 7. They assume that the Si III] line emission comes from the pre-shock, in a gas that moves at ~ 300 km s $^{-1}$. The fast moving gas produces the extended wings in the lines. They argue that a tilted dipole can reproduce the shape of the line, assuming that it is the result of the orientation of the accretion region with respect to the observer. In Figure 19 we compare the red lines of Si IV and C IV (without H₂) with the Si III] line for these two stars. As can be seen, the centroids and widths of both lines are similar, which supports the hypothesis that the main contribution to the Si IV and C IV lines comes from the same region.

Lamzin (2000c) argue that to reproduce the Si III] line for RU Lup one needs an inclined rotation axis for the star but symmetric accretion zones aligned with the disk axis. As they recognize, it is not clear what the physical plausibility of this model is. To reproduce the observed profiles, their models assume that the inclination of the observer is 10 degrees for RU Lup and 12 degrees for RY Tau. Observationally, however, the inclination of RY Tau is likely to be much larger, close to 90 degrees, given that $v \sin i = 52$ km s $^{-1}$ and $P_{\text{rot.}} = 5.6$ days.

While these geometrical models that assume that the lines are formed in the pre-shock can produce symmetric, redshifted, and slightly blueshifted profiles, the strong emission at ~ -300 km s $^{-1}$ in DG Tau or the episodic emission at the red of DR Tau must be produced by a different mechanism. DG Tau is almost pole-on and it is known to have a strong jet, in which velocities as large as 300 km s $^{-1}$ have been observed (Bacciotti et al. 2000). However, wind models predict (Shu et al. 1994) that its temperature is at most 10000 K close to the launching point, which rules out the base of the wind as the source of the C IV emission. Models by Goodson, Böhm, & Winglee (1999) show that fast episodic emission of very hot plasma in the magnetosphere of a CTTS is likely to occur, due to entangling and reconnection of the stellar magnetic field. It is possible that this is what we are observing in the case of DG Tau and DR Tau.

A direct measurement of the physical conditions in the emission line region is provided by the line ratios. Given that the f-value of the blue doublet member is twice that of the red doublet member (for both C IV and Si IV), optically thin (or effectively thin) conditions imply that the blue member should be twice as strong as the red member. Table 7 shows the ratios of each doublet member for Si IV and C IV. T Tau and HBC 388 are the only stars for which Si IV may indicate optically thin emission. For all stars, except RU Lup and DR Tau (9/7/95) (and perhaps DG Tau), the C IV ratios indicate optically thin emission. For comparison, the SUMER Atlas for the Sun shows an almost perfect 2-to-1 ratio between the

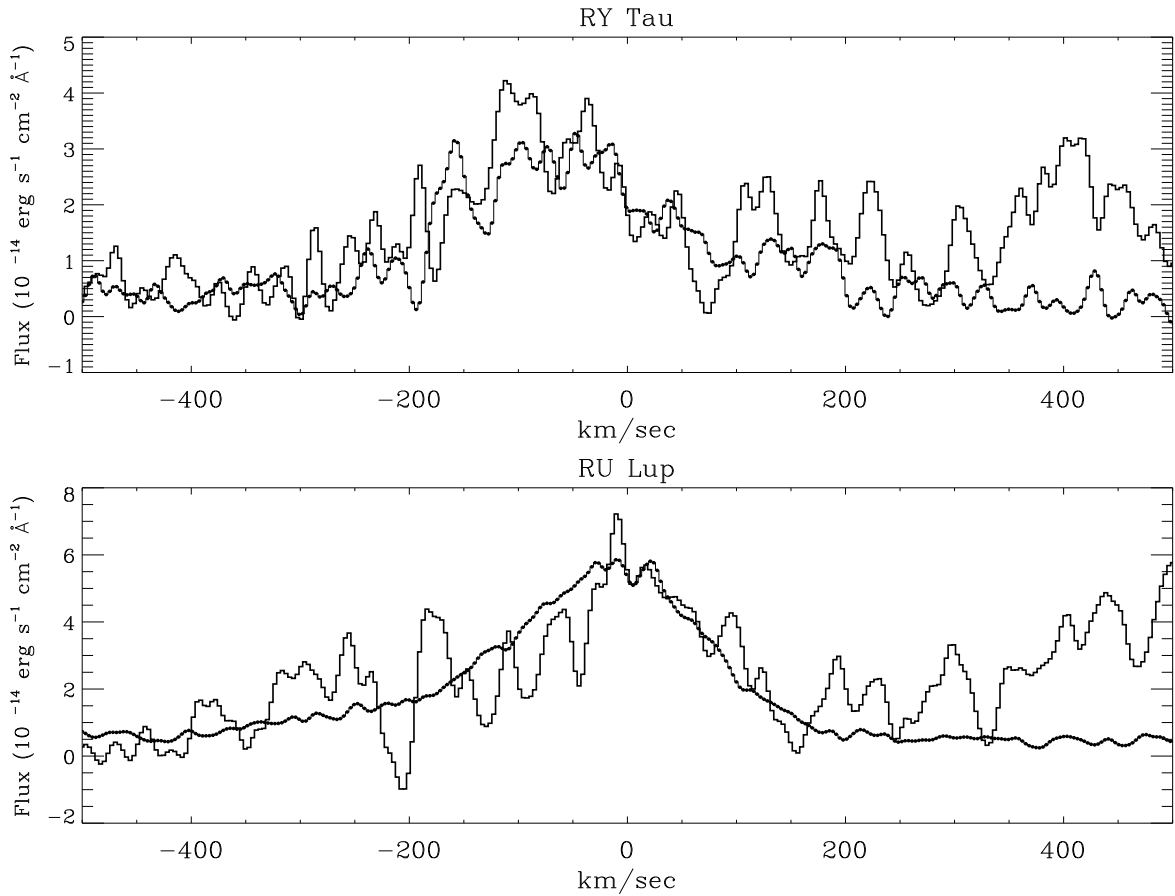


Fig. 19.— Comparison between the red members of C IV (thick line) with the Si III] (1892 Å) line (thin dotted line). For RY Tau, we have scaled the observed Si III] profile by 0.25. Lamzin (2000c) argue that the width of Si III] is due only to kinematic broadening.

blue and red members of the C IV and Si IV doublets.

Almost certainly, the radiative precursor is effectively thin in C IV and Si IV (Lamzin 1998). Therefore, Si IV cannot be formed here. Due to the rapid motion of the gas flow in the post-shock, it is possible that these hot lines are formed close to the star, at temperatures of the order of $\sim 10^4$ K. At such temperatures, He and H are not fully ionized and may provide enough opacity to significantly absorb Si IV. In this case, however, one is left with the problem of explaining the widths of the lines.

In summary, while the relative ratios of the resonance doublets are consistent with the lines being formed after the accretion shock, their widths are consistent with formation in the radiative precursor. The centroids are difficult to understand assuming formation in one region or the other only. Models of formation before the shock have to explain the nearly symmetric appearance of the doublets in the face of multiple geometric configurations. Models of formation after the shock have to explain the line width.

5. Conclusions

We have analyzed GHRS data of eight CTTS and one WTTS. The GHRS data consists of spectral ranges 40 Å wide centered on 1345, 1400, 1497, 1550, and 1900 Å. These UV spectra show strong Si IV, and C IV emission, and large quantities of sharp (~ 40 km s $^{-1}$ in average) H₂ lines. In a companion paper we analyze the Mg II resonance doublet centered on 2800 Å.

All the H₂ lines belong to the Lyman band (transitions from $B^1\Sigma_u^+$ to $X^1\Sigma_g^+$). We identify seven different routes, where the lines in the same route all come from the same upper level. All the observed lines are single peaked and we verify that they are all optically thin.

We do not observe any correlation between the intensity of the measured H₂ lines, their center, and their FWHM with each other or with the inclination of the systems. The lack of correlation between line flux and inclination suggests that the gas responsible for the H₂ emission is not limited to the disk. We observe that the average of the centroids for all the lines measured in each star is blueshifted. Centering errors in the spectrograph may produce shifts from star to star of up to 20 km s $^{-1}$. Also, an asymmetric, non-uniform, spatially-extended distribution would produce velocity shifts. However, it would be surprising if all the shifts were to be in the same direction. Line widths vary from about 20 to 60 km s $^{-1}$. Turbulence, or inhomogeneities in the extended spatial distribution of H₂ in TTSs (as has been observed in T Tau) may be responsible for these widths.

Table 7. Ratios of Transition Line Doublets

Name	Si IV	C IV
BP Tau	1.4 ± 0.5	2.0 ± 0.2
T Tau	1.7 ± 0.3	2.4 ± 0.4
DF Tau	...	2.13 ± 0.3
RW Aur	0.8 ± 0.1	1.6 ± 0.9
DG Tau	...	1.6 ± 0.3
DR Tau	...	$1.0 \pm 0.4, 1.4 \pm 0.2$
RY Tau	...	1.8 ± 0.5
RU Lup	1.3 ± 0.1	1.2 ± 0.2
HBC 388	1.8 ± 0.7	1.9 ± 0.5

Note. — All the ratios have been calculated once the contribution of H₂ has been subtracted

Regarding the origin of the emission, if H_2 is formed in the surface layers of the disk, the observed profiles should be double peaked. The GHRS resolution is such that we should be able to observe double peaked profiles from within $\sim 10(M/0.5M_\odot) \sin^2 i$ AU of the central star, where M is the mass of the star and i is the inclination. All the observed profiles are single peaked, and we do not observe any correlation of width and inclination. Together with the fact that the averages of the lines for each star are blueshifted, this suggests that H_2 is formed in a material moving towards the observer, i.e. an outflow. On the other hand, it is not difficult to imagine circumstances in which this is not true: the H_2 emission comes from a large disk region, the blueshift of the lines is accidental, due to either centering errors (which would have to be in the same direction in all the stars!) or asymmetric extended H_2 emission.

We interpret the emission in H_2 as being due to fluorescence mostly by $\text{H}_{Ly\alpha}$: this line is one order of magnitude stronger than other atomic lines in the spectra. Furthermore, we can track every observed H_2 line to an excitation line within 1000 km s^{-1} of $\text{H}_{Ly\alpha}$. Fluorescent H_2 lines in CTTSs have already been reported widely in the literature (e.g. Brown et al. 1981, 1984; Valenti et al. 2000). The observed fluorescent routes are excited from levels $N(v'',J'')=N(2,0)$, $N(2,1)$, $N(2,2)$, $N(2,5)$, $N(2,6)$, and $N(1,13)$. None of the observed routes is excited from the blue wing of $\text{H}_{Ly\alpha}$, even though there are strong transitions present there that would produce fluorescent cascades strong enough to be seen in our spectra. Higher signal-to-noise data would be necessary before we can say whether this is due to the exotic (i.e. non-thermal) level populations or to the fact that absorption of $\text{H}_{Ly\alpha}$ photons by H_2 occurs relatively far from the star, where the blue wing of $\text{H}_{Ly\alpha}$ has already been absorbed by the wind.

We use previous measurements of the $\text{H}_{Ly\alpha}$ flux by IUE to obtain estimates of the column densities and optical depths of the states from which the excitation occurs. This is an uncertain process given the low signal-to-noise of the IUE spectra in this region and the low number of them. We assume that $\text{H}_{Ly\alpha}$ can be modeled by a Gaussian, that the strength is 30 times larger than the blue member of the C IV doublet (valid for RU Lup), and that the Gaussian has $\sigma = 1.2 \text{ \AA}$ (valid for TW Hya). From these assumptions we obtain optical depths of the exciting transitions (~ 1 or less) and column densities of the levels from which the transitions originate (10^{12} to 10^{15} cm^{-2}). Errors in the intensity of the $\text{H}_{Ly\alpha}$ flux will change the absolute column densities but not their relative values. We conclude that the populations are far from being in thermal equilibrium, an important constraint in modeling efforts. This conclusion is independent of the exact line shape (Gaussian or Voigt) as long as the $\text{H}_{Ly\alpha}$ is centered at rest wavelengths and its intensity decreases to the red. A comparison with ISO observations by van den Ancker et al. (1999) shows that our results are within the parameter region predicted by a thermal gas at 1500 K with a total column density of

$2 \times 10^{18} \text{ cm}^{-2}$ (derived from far IR lines). Obviously, this coincidence is not incompatible with the lack of a thermal distribution for upper levels of H₂: a mechanism that produces a thermal distribution in the lower levels does not necessarily have an effect in the upper levels.

The main weakness of this approach is that the IUE observations show that H_{Lyα} is very redshifted, perhaps because its blue wing has been absorbed by an outflow or by the ISM (which means that the flux absorbed by H₂ is probably 3-4 times larger as the one we use). What the exact shape of the line producing the excitation of H₂ is, we cannot tell from these data. The fact that all the observed routes are excited from transitions to the red of the rest wavelength of H_{Lyα} suggests that at least some absorption has already taken place when the line radiation arrives to the location of H₂. What we have shown is that if H_{Lyα} can be approximated by a Gaussian centered at 1215.67 Å, the populations of the H₂ states that absorb H_{Lyα} are not thermal. If one accepts these assumptions, our results firmly suggest that better models of excitation of H₂ by radiation are needed, given that even at $v''=2$ the levels do not have a thermal population.

If the ions are collisionally formed, the C IV and Si IV lines arise in hot (10^5 K) regions. In the past, analyses of these lines have been carried out using the low resolution spectra provided by IUE. In principle, these kind of analyses have the problem that there are strong H₂ lines whose positions coincide with those of the transition lines. In this work we correct for H₂ emission by using other lines from the same fluorescent route to calculate the contribution to the transition lines (as we have confirmed that the H₂ lines are optically thin). In this way, we obtain unblended profiles of the C IV and Si IV lines, and conclude that the contribution of the H₂ lines to the profiles is less than 10% and that the variability of the fluxes is dominated by variability in C IV and Si IV.

After subtracting the H₂ contribution, we show that the shape of the C IV lines is the same as that of the Si IV lines (with the exception of RW Aur), and that their fluxes are linearly correlated in log space. In spite of this correlation, a wide variation is observed in the ratio of C IV to Si IV flux. It is not clear what is the origin of such variation. For RW Aur, Errico et al. (2000) argues that strong Fe II absorptions are present in the C IV and Si IV profiles. We do not see any example of these absorptions in any other star.

The profiles have full-widths at half-maxima that vary from 200 to 300 km s⁻¹, and a wide array of centroids (blueshifted, centered, redshifted). In particular, blueshifted emission at $\sim -300 \text{ km s}^{-1}$ is observed in the C IV lines of DR Tau and DG Tau. In the first star, the emission is episodic, as it is shown by the two separate epochs of observations in our data. These blueshifted emissions are perhaps evidence of reconnection processes in the magnetosphere that behave as a coronal wind, given that the standard magnetocentrifugally

driven T Tauri wind is expected to be too cold to produce this kind of emission. According to Shu et al. (1994) such reconnection events occur as a consequence of mismatches between the rotation rate of the star and the point at which the disk is truncated, and they may be the cause of much of the variability observed in TTS spectra. They have been modeled in detail by Goodson et al. (1999). Evidence from hot episodic emission has been observed in H α (Alencar et al. 2001) and in He I (Beristain, Edwards, & Kwan 2001).

We observe a correlation between the C IV line and the H $_2$ emission. Such correlation has also been observed by Johns-Krull et al. (2000) for a large sample of CTTSs. It is surprising given that the physical conditions of H $_2$ are different for each star and indicates that the H $_2$ emission is limited by the excitation mechanism and not by the H $_2$ population. This is a useful fact that any modeling attempt should take into account. For the stars of this paper, the observed C IV and Si IV lines are most likely the result of accretion-related (as opposed to chromospheric) processes. If we assume that the transition region emission of our CTTSs is like that of HBC 388 (a WTTS), we conclude that the dominant contribution to the C IV line flux comes from accretion related processes. Our results also suggest that for accretion rates of the order of $10^{-9} M_{\odot}/\text{yr}$ most of the line flux in C IV should come from the stellar chromosphere. A correlation is also observed (albeit not a very strong one) between the C IV line flux and the accretion rate. The lack of a strong correlation is not a surprise: in addition the fact that our sample is very small, accretion rates are measured at one point in time and are known to change (Ardila & Basri 2000), as are the measured fluxes. Without a theory of the behavior of the transition region lines as a function of accretion rate is not clear what the correlation presented here (or the more extensive one obtained by Johns-Krull et al. 2000) is really indicating.

While it seems clear that the Si IV and C IV lines are related to the accretion shock formed when the gas flow impacts the stellar surface, the exact region of formation remains a mystery. The shape and centroid of C IV is similar to that of the Si III] line, believed to be emitted from the radiative precursor of the shock (Lamzin 2000c). Formation in the pre-shock may explain the widths of the lines as being due to the projection of the accretion ring in the stellar surface with respect to the observer. Emission from this region would preferentially produce redshifted profiles, as the gas flow is still moving at almost free-fall velocities. However, a sizable fraction (4 out of 8) of the observed profiles have zero velocity centroids, a remarkable statistical coincidence if the position of the centroids is due to the apparent position of the emitting region in the stellar surface. Furthermore, while C IV lines tend to be optically thin, the Si IV profiles are not (the exceptions are HBC 388 and T Tau, for which the flux ratios indicate that the Si IV profiles are optically thin). Models of the radiative precursor indicate that this should be effectively thin in both lines.

If most of the emission is originated in the post-shock, line formation will occur close to the star, where the gas has temperatures of $\sim 10^4$ K. At this point, the column is starting to become optically thick to its own radiation and so emission from the region is consistent with the observed flux ratios. On the other hand, such region will produce centered, narrow profiles, unlike the observed ones.

Multiple emission regions are possible. The C IV and Si IV lines of BP Tau can be decomposed in multiple Gaussian components, with a broad (~ 300 km s $^{-1}$) and a narrow component (~ 100 km s $^{-1}$). For DF Tau, the only star in which the signal-to-noise is large enough, we observe a third component, with ~ 50 km s $^{-1}$ width. This suggests that the emission in the hot lines may come from more than one region. However, all components have velocities near zero. As suggested above, simultaneous formation in the pre- and post-shock should produce widely different velocity centroids.

The study of these ultraviolet ranges provide us with yet another window into which to look at T-Tauri phenomena. What these analyses show is that there is still a lot of work to be done in the theoretical front before we can understand the innermost regions of TTS. Observationally too, it is clear that high resolution spatial and spectral observations with good time coverage are necessary before a more careful model of the region can be attempted.

This paper is based on observations made with the NASA/ESA *Hubble Space Telescope*, obtained at the Space Telescope Science Institute, which is operated by the Association of Universities for Research in Astronomy, Inc., under NASA contract NAS 5-26555. DRA and GB acknowledge support from the National Science Foundation (grant ASI952872) and NASA (grant NAG5-3471). FMW acknowledges support through NASA grants NAG5-1862, STScI-GO-5317-0193A, STScI-GO-058750294A, and STScI-GO-3845.02-91A to SUNY Stony Brook. CMJK acknowledges support through NASA grant NAG5-8209.

We thank G. Herczeg and J. Linsky for supplying us with their STIS TW Hya spectrum in advance of publication. We also thank D. Hollenbach, M. McMurry, J. Black, and C. Jordan for fruitful discussions on molecular hydrogen.

REFERENCES

Abgrall, H., Roueff, E., Launay, F., Roncin, J. Y., & Subtil, J. L. 1993, A&AS, 101, 273
Alencar, S. H. P. & Basri, G. 2000, AJ, 119, 1881
Alencar, S. H. P., Johns-Krull, C. M., & Basri, G. 2001, submitted to ApJ

Ardila, D. R. and Basri, G. 2000, *ApJ*, 539, 834

Arnaud, M. & Raymond, J. 1992, *ApJ*, 398, 394

Ayres, T. R., Marstad, N. C., & Linsky, J. L. 1981, *ApJ*, 247, 545

Bacciotti, F., Mundt, R., Ray, T. P., Eislöffel, J., Solf, J., & Camezind, M. 2000, *ApJ*, 537, L49

Bartoe, J. . F., Brueckner, G. E., Nicolas, K. R., Sandlin, G. D., Vanhoosier, M. E., & Jordan, C. 1979, *MNRAS*, 187, 463

Beristain, G., Edwards, S., & Kwan, J. 2001, *ApJ*, 551, 1037

Black, J. H. & van Dishoeck, E. F. 1987, *ApJ*, 322, 412

Blackwell, J., Shore, S., Robinson, R., Feggans, K., Lindler, D., Malumuth, E., Sandoval, J., & Ake, T. 1993, *A User’s Guide to the GHRS Software* (Baltimore:GSFC)

Blondel, P. F. C., Talavera, A., & Djie, H. R. E. T. A. 1993, *A&A*, 268, 624

Brandt, J. C., et al. 1994, *PASP*, 106, 890

Brandt, J. C., et al. 1993, *AJ*, 105, 831

Brown, A., de M. Ferraz, M. C., & Jordan, C. 1984, *MNRAS*, 207, 831

Brown, A., Jordan, C., Millar, T. J., Gondhalekar, P., & Wilson, R. 1981, *Nature*, 290, 34

Calvet, N. & Gullbring, E. 1998, *ApJ*, 509, 802

Calvet, N., Hartmann, L., Hewett, R., Valenti, J. A., Basri, G., & Walter, F. 1996, in *ASP Conf. Ser. 109: Cool Stars, Stellar Systems, and the Sun*, ed. R. Pallavicini & A. K. Dupree (San Francisco: ASP), p.419

Curdt, W., Brekke, P., Feldman, U., Dwivedi, B. N., Schüle, U., & Lemaire, P. 2000, in *Submitted to A&A Supplement*.

Errico, L., Lamzin, S. A., & Vittone, A. A. 2000, *A&A*, 357, 951

Gahm, G. F., Petrov, P. P., Duemmler, R., Gameiro, J. F., & Lago, M. T. V. T. 1999, *A&A*, 352, L95

Ghez, A. M., Neugebauer, G., & Matthews, K. 1993, *AJ*, 106, 2005

Ghez, A. M., White, R. J., & Simon, M. 1997, *ApJ*, 490, 353

Gomez de Castro, A. I. & Lamzin, S. A. 1999, *MNRAS*, 304, L41

Gomez de Castro, A. I., Lamzin, S. A., & Shatskii, N. I. 1994, *Astronomy Reports*, 38, 540

Goodson, A. P., Böhm, K., & Winglee, R. M. 1999, *ApJ*, 524, 142

Gullbring, E., Calvet, N., Muzerolle, J., & Hartmann, L. 2000, *ApJ*, 544, 927

Gullbring, E., Hartmann, L., Briceno, C., & Calvet, N. 1998, *ApJ*, 492, 323

Hartigan, P., Edwards, S., & Ghandour, L. 1995, *ApJ*, 452, 736

Hartmann, L., Stauffer, J. R., Kenyon, S. J., & Jones, B. F. 1991, *AJ*, 101, 1050

Heap, S. R. et al. 1995, *PASP*, 107, 871

Herbig, G. H. & Bell, K. R. 1988, Catalog of emission line stars of the orion population (Santa Cruz: Lick Observatory)

Herbst, T. M., Robberto, M., & Beckwith, S. V. W. 1997, *AJ*, 114, 744

Herczeg, G. H., Linsky, J. L., Valenti, J. A., & Johns-Krull, C. M. 2001, in Submitted to *ApJ*

Hughes, J., Hartigan, P., Krautter, J., & Kelemen, J. 1994, *AJ*, 108, 1071

Johns-Krull, C. M., Valenti, J. A., Hatzes, A. P., & Kanaan, A. 1999, *ApJ*, 510, L41

Johns-Krull, C. M., Valenti, J. A., & Linsky, J. L. 2000, *ApJ*, 539, 815

Jordan, C., Brueckner, G. E., Bartoe, J. . F., Sandlin, G. D., & Vanhoosier, M. E. 1978, *ApJ*, 226, 687

Kurt, V. G. & Lamzin, S. A. 1995, *Astronomy Reports*, 39, 322

Lamzin, S. A. 1998, *Astronomy Reports*, 42, 322

—. 2000a, *Astronomy Letters*, 26, 225

—. 2000b, *Astronomy Letters*, 26, 589

—. 2000c, *Astronomy Reports*, 44, 323

Lamzin, S. A., Bisnovatyi-Kogan, G. S., Errico, L., Giovannelli, F., Katysheva, N. A., Rossi, C., & Vittone, A. A. 1996, *A&A*, 306, 877

Lamzin, S. A., Vittone, A. A., & Errico, L. 2001, *Astronomy Letters*, 27, 313

Leinert, C., Zinnecker, H., Weitzel, N., Christou, J., Ridgway, S. T., Jameson, R., Haas, M., & Lenzen, R. 1993, *A&A*, 278, 129

Martin, P. G. & Mandy, M. E. 1995, *ApJ*, 455, L89

McMurry, A. D., Jordan, C., & Carpenter, K. G. 1999, *MNRAS*, 302, 48

Muzerolle, J., Hartmann, L., & Calvet, N. 1998, *AJ*, 116, 455

Petrov, P. P., Gahm, G. F., Gameiro, J. F., Duemmler, R., Ilyin, I. V., Laakkonen, T., Lago, M. T. V. T., & Tuominen, I. 2001, *A&A*, 369, 993

Preibisch, T. & Smith, M. D. 1997, *A&A*, 322, 825

Sandlin, G. D., Bartoe, J. . F., Brueckner, G. E., Tousey, R., & Vanhoosier, M. E. 1986, *ApJS*, 61, 801

Sartoretti, P., Brown, R. A., Latham, D. W., & Torres, G. 1998, *A&A*, 334, 592

Shu, F., Najita, J., Ostriker, E., Wilkin, F., Ruden, S., & Lizano, S. 1994, *ApJ*, 429, 781

Stapelfeldt, K. R. et al. 1998, *ApJ*, 508, 736

Thi, W., van Dishoeck, E. F., Blake, G. A., van Zadelhoff, G., & Hogerheijde, M. R. 1999, *ApJ*, 521, L63

Thiebaut, E., Balega, Y., Balega, I., Belkine, I., Bouvier, J., Foy, R., Blazit, A., & Bonneau, D. 1995, *A&A*, 304, L17

Valenti, J. A., Basri, G., Walter, F., Hartmann, L., & Calvet, N. 1993, *BAAS*, 183, 4007

Valenti, J. A., Johns-Krull, C. M., & Linsky, J. L. 2000, *ApJS*, 129, 399

van den Ancker, M. E., Wesselius, P. R., Tielens, A. G. G. M., van Dishoeck, E. F., & Spinoglio, L. 1999, *A&A*, 348, 877

van Dishoeck, E. F., Thi, W. F., Blake, G. A., Mannings, V., Sargent, A. I., Koerner, D., & Mundy, L. G. 1997, *Ap&SS*, 255, 77

Walter, F. M., Brown, A., Mathieu, R. D., Myers, P. C., & Vrba, F. J. 1988, *AJ*, 96, 297

Walter, M. & Liu, Y. 1998, in ASP Conf. Ser. 143: The Scientific Impact of the Goddard High Resolution Spectrograph, ed. J. C. Brandt, T. B. Ake, & C. C. Petersen, 360

Weintraub, D. A., Kastner, J. H., & Bary, J. S. 2000, *ApJ*, 541, 767

Wolk, S. J. & Walter, F. M. 1996, *AJ*, 111, 2066